Third-sound propagation in thick films of superfluid ^{4}He

H. W. Jackson and P. V. Mason
Jet Propulsion Laboratory, California Institute of Technology, Pasadena, California 91109
(Received 25 October 1989)

Atkins' theory of third sound in thick films of superfluid helium-4 has been extended to include a heat source for excitation. Calculations based on the resulting equations reveal the physical structure of third sound, and it is shown that this structure is not consistent with the standard description, which is based largely on qualitative analysis. Calculations also predict the existence of solitary waves, a new type of third-sound signal excited by very short heat pulses. They have not yet been observed experimentally. Additional calculations show in detail how such waves are generated at a localized heater. Results of various observations of third sound reported in the literature during the past 30 years are studied with the aid of the more complete theory. This study indicates a number of factors that complicated interpretation of the observations and suggests that large discrepancies between theoretical and experimental results that have been reported may be largely due to inappropriate comparisons. Conditions favorable for observing individual normal modes of third sound, where interpretation of the results should be particularly transparent, are investigated and could serve as a useful basis for new experiments. A direct method for accurately measuring the vaporization coefficient utilizing results in this article is described. This coefficient is of central importance in accounting for third-sound attenuation. Failure to account for that attenuation was believed to be a major deficiency of the theory in the past. Also, an energy conservation law is derived and then used to help explain the physical nature of third-sound attenuation.

I. INTRODUCTION

Third sound is a long-wavelength surface disturbance on a liquid-helium film in which the normal component of the fluid remains stationary while the superfluid component oscillates mainly in a direction parallel to the wall. This motion produces ripples at the free surface of the film similar to water waves in a shallow channel.

Atkins[1] published the seminal paper on third sound in 1959. Despite the impressive insight and relatively simple concepts underlying Atkins' original theory, the understanding of these surface waves is still incomplete and an explanation of certain features that have been observed experimentally still stands as a challenge to researchers today. Progress in this effort promises great reward, for history shows that third sound is a highly valuable tool in probing a variety of fundamental properties of liquid-^{4}He films. A number of examples of such properties will be enumerated and discussed later in this introduction. Sharpening the theory of third sound will open up new uses for it as a probe. Furthermore, it seems likely that some of the shortcomings of the existing theory will find explanation in mechanisms and phenomena that are of considerable interest in their own right.

We have extended Atkins' basic theory[1,2] to include a source for heat that can excite third sound. Then we have applied the resulting equations to a one-dimensional model obeying periodic boundary conditions. Such a model can represent a variety of experimentally important configurations, including an annular track, a cylinder, and a flat plate, provided that the heater and detector are arranged appropriately. General formulas for solutions of those equations have been found which give a complete description of third-sound waves in terms of displacement of the film surface, superfluid velocity, and temperature change as functions of space and time. Algebraic expressions for quantities that occur in the general formulas are found for special excitation signals.

Calculations based on those new results are then used to elucidate a number of features of third sound.

One of the most interesting new phenomena revealed by the theoretical calculations is a solitary wave, basically a single ripple on the film surface, that can be excited by a very short pulse at a localized heater and which subsequently propagates with almost constant velocity. (The term "solitary wave" used here refers to a propagating disturbance accounted for by linearized equations, like those in our treatment. "Solitary wave" should not be confused with "soliton," which is a term usually reserved for certain disturbances accounted for by a nonlinear theory.) Under some conditions the waves travel with little distortion, but under certain conditions the wave form changes substantially as it travels along the surface. The origin of the distortion of the shape is found to be significantly different from the well-known mechanism of wave-packet spreading in a dispersive medium. The processes involved in formation of the wave at the heater are studied and evolution of the surface disturbance in space and time is exhibited. Correlations in the space and time distributions of surface displacement, temperature change, and superfluid velocity are found to be quite different from those expected on the basis of earlier discussions of the structure of third-sound waves. This discrepancy was found not only for solitary waves, but

for all of the wave forms that we have investigated so far.

Calculations based on the new formulas have been used to help analyze and explain experimental results that other researchers have reported in the literature. Also, calculations have been made to aid in the search for methods and arrangements that are particularly favorable for observation of third sound in its most elementary form, that is, as an excitation of an individual normal mode, or resonance. In addition, calculations have been made to study uniform evaporation of a film as a means of directly measuring a coefficient of vaporization that is of major importance in the theory.

The numerical results show that contributions to the surface disturbance by the normal mode at wave number $k=0$ can be important in some instances and must have affected certain earlier experimental observations. Those contributions have not been taken into account in previous treatments of third sound. Furthermore, in the cases we have examined so far, more than one normal mode with finite wave numbers was usually appreciably excited, a complication that has not been taken into account previously in the interpretation of experimental data.

We examine the working hypothesis that the basic theory of third sound developed by Atkins is fairly accurate when it is extended to include a heat source for excitation. This hypothesis is in conflict with the current interpretation of a large body of existing experimental data, especially that part which relates to attenuation. Our study in this paper leads us to the conclusion that Atkins' theory may be correct, at least for some ranges of temperature and film thickness, and that it would be highly desirable for certain additional experiments to be carried out to explore this further.

Since dissipative coefficients such as viscosity and thermal conductivity do not appear explicitly in Atkins' theory, it may seem puzzling that third-sound waves are nevertheless predicted to be attenuated. Bergman[3] asserted that, for thick films, attenuation of third sound is associated with evaporation and condensation at the interface of the liquid with the vapor. For thin films Bergman has shown that other effects are also important in attenuation. Of course, in principle, evaporation and condensation can be reversible processes; therefore, it is not obvious that they should contribute to attenuation, which is expected to reflect conversion of mechanical energy into heat. This matter is treated in the Appendix, where a law for energy conservation is derived. It is shown there that attenuation is associated with evaporation and condensation at the film surface and with the fountain effect term in the equation of motion for the superfluid. The combination of these effects produces a small correction to the latent heat that depends on the direction of mass flow between the film and the vapor. This results in an excess heat flow that is unidirectional from the film to the vapor. This loss of energy from the film accounts for the dominant part of third-sound attenuation in this theory.

Next, some of the earlier work on third sound will be reviewed with a brief commentary as a means of clarifying ideas discussed above and explaining motivations for new developments in this paper.

A. Overview of studies of basic properties of third sound

The theory of third sound developed by Atkins[1,2] is based on the two-fluid model for the ^{4}He film in an external potential. That potential is due to the van der Waals attraction of the helium atoms to the substrate. In terrestrial laboratories there is also a contribution to the potential due to gravity. Boundary conditions are specified in a simplified form such that it is not necessary to deal with equations of motion and heat flow in the neighboring substrate and vapor.

Third-sound waves were detected for the first time by Everitt, Atkins, and Denenstein.[4] They found that the measured phase velocity was in semiquantitative agreement with Atkins' theoretical predictions. In that experiment, as well as in more recent investigations,[5,6] the observed phase velocity agrees with theory to within a factor of 2 or better. The discrepancies in phase velocity are extremely small for films thicker than about 15 atomic layers at low temperatures. These discrepancies increase as the thickness decreases or as the temperature rises toward the λ point for the bulk liquid. For films thicker than about 35 atomic layers, agreement is good below about 1.7 K but deteriorates as T_λ is approached.

General agreement of the observed phase velocity with theoretical predictions helps to instill confidence in the validity of Atkins' theory. Therefore, it is surprising that, in some cases, measured values of attenuation of third sound were found to be as much as 2 or 3 orders of magnitude greater than predicted.[2,5,7–9] It seems worth noting, however, that the theory predicts only slight dispersion for third sound, so that phase velocity is almost the same as group velocity and can be measured simply and accurately by time-of-flight methods. On the other hand, attenuation affects the shapes and amplitudes of the waves and extraction of numerical values from observed results involves assumptions about more intricate details of the theory.

In the earliest measurements[5] it was recognized that part of the disagreement in the case of attenuation may be associated with lack of reproducibility in the observed results from day to day, but experiment still appeared to indicate the existence of a real attenuation much larger than anything predicted in the original theory. In that work, third-sound waves on a flat rectangular surface were studied. Waves were excited by a chopped infrared beam that produced heating along a narrow line and were detected by an optical method. Data that could be regarded as snapshots of the film surface at different instants of time were presented in graphical form, and values for attenuation were extracted from them.

In Sec. III B of this paper, we present detailed calculations and analysis of those experiments based on our more complete theory. The results indicate that the huge discrepancies for attenuation reported earlier are at least in part due to inappropriate comparisons between theory and what was actually observed.

A later experiment by Wang and Rudnick[8] investigated attenuation of third sound on the outer surface of a horizontal glass cylinder about 1 cm in diameter and 3.2 cm long. Heating of a narrow strip of a metallic thin film

excited the third sound, which was then detected by measuring the temperature oscillations of the wave using an aluminum thin-film strip operating near its superconducting transition. A single-cycle sine burst electrical signal produced the third-sound pulse, which travelled in both directions around the cylinder. Values of attenuation inferred from the observations exhibited a minimum as a function of film thickness near 25 Å for a temperature near 1.1 K, and near 55 Å for a temperature close to 1.7 K. Except for a small range of thicknesses near the minimum, the experimental attenuation is much greater than predicted by Atkins' theory, as much as 2 or 3 orders of magnitude greater for the thickest films studied, of about 300 Å.

In Sec. III C we analyze details of that experiment and present results based on our new theoretical formulas. We conclude that, at least for the thickest films studied, proper interpretation of the experiments would be complicated by two effects that account in part for the discrepancies. First, distortion of the third-sound signals was introduced by variations in the equilibrium thickness of the film due to gravitational effects. Second, the observed waves were not associated with single normal modes with exponential decay, as they assumed. Portions of the signals they observed involved many normal modes according to our calculations. Therefore, we believe that their inference that the theory is in gross conflict with their observations is open to question and that this matter should be studied further.

In a series of papers, Bergman[3,7,10] analyzed the theory of third sound in great detail, taking into account equations of motion and heat flow in the substrate and vapor as well as in the film. For thick films the results of his analysis agreed closely with Atkins' theory,[1,2] differing mainly just in the value of a coefficient of vaporization γ which occurs in formulas for attenuation. Bergman[3] found $\gamma=\frac{16}{9}$ while Atkins assumed $\gamma=1$. This general agreement seemed to validate Atkins' theory, but it added to the mystery of the poor agreement between theory and experiment on attenuation in thick films. However, it should be mentioned that other researchers have reported a wide range of values of an accommodation coefficient that sometimes has been regarded to be the same as γ. In Sec. III D of this paper we review this matter. Then we discuss a new method for directly measuring γ that involves uniform evaporation of a film and utilizes formulas that we have derived.

For thin films, Bergman found that Atkins' theory was not accurate in certain respects. For example, Bergman[3,7,10] found the frequency dependence of attenuation to be $\omega^{1/2}$ there rather than ω^2 as in Atkins' theory, which is only appropriate for thick films according to Bergman.[3] Bergman[3,7] found that the transition from thick- to thin-film behavior occurred in the neighborhood of 100 Å, although in the literature[2] 100 atomic layers, about 360 Å, had frequently been regarded on theoretical grounds as the thickness where the transition occurs.

Measurements of attenuation by Wang and Rudnick[8] were in better numerical agreement with Bergman's theory when the films were thin than when they were thick, although the discrepancies were substantial even in the former case.

Ratnam and Mochel[9,11,12] performed a series of experiments on thin films in a closed resonating cavity for third sound in which they found evidence that single resonances at finite wave numbers were excited in some instances. Their measured values of attenuation[9] seemed at first to agree with Bergman's theory. Bergman[7] later analyzed their experiments in detail and found that the attenuation values predicted by theory were sometimes 2 or 3 orders of magnitude less than the measured values. Bergman did not take into account the $k=0$ terms, and these terms must have affected the observed signals. However, it seems unlikely that the $k=0$ terms account for the large discrepancy in the experimental configuration used by Ratnam and Mochel. An important mechanism that can cause attenuation has been omitted in the existing theory for thin films.

A number of attenuation mechanisms have been identified and studied and have been reviewed in the literature.[2,7,13] However, none so far has been shown to account for the large discrepancy between theoretical and experimental results for either thick or thin films.

B. Review of uses of third sound as a probe of superfluid helium films

Atkins[1,2] developed the theory of third sound in response to an idea proposed earlier by Kuper[14] that the critical velocity in flowing films of helium could be explained by applying Landau's criterion[14–16] to an elementary excitation spectrum for surface waves. Subsequent experimental studies[2,17] were interpreted as demonstrating that Kuper's hypothesis was not correct. Nevertheless, from the very outset third sound was recognized as a valuable probe of fundamental properties of superfluid ^{4}He.

This point is illustrated further in one of the highlights[18] of third sound studies, where it was unexpectedly found that third sound abruptly ceased to propagate for film thicknesses less than a certain threshold if the temperature was fixed at a sufficiently low value. Those observations later found explanation in theoretical[19–22] and experimental[23] studies of vortex-antivortex binding as a mechanism underlying the onset of superfluidity in ^{4}He films. The vortices that are postulated in these theories to exist even below the transition temperatures for thin films should scatter third sound and so attenuate it. These vortices could be responsible for the large discrepancy between theoretical and experimental results for attenuation in thin films mentioned earlier. Generazio and Reed[13] have called attention to the need for further work on this problem.

The Doppler shift of third sound in flowing ^{4}He films has also been a useful tool in exploring basic properties of ^{4}He films. This effect has been used to help confirm the existence of persistent currents in ^{4}He films and to measure the velocity of flowing films.[24] Other interesting applications of third sound were concerned with measuring the thickness of films and with studying the existence of Kontorovich thinning of flowing films.[17,25,28]

C. Commentary on the new developments and their implications

So far the usefulness of third sound as a probe has relied heavily on the properties of the phase velocity, which is fairly well understood. When attenuation is understood better, additional phenomena can be investigated with its help. New developments in this paper shed light on some of the previously unresolved problems in understanding third sound, including its attenuation.

It would be highly desirable to have additional measurements to compare directly with predictions of the new analysis that takes into account all resonances simultaneously, including the $k=0$ terms. In the case of thick films, the temperature range below about 1.8 K is where we believe good agreement is most likely to be found. Favorable results there would then establish a reliable basis for studying the possibility that additional mechanisms that affect attenuation and velocity of third sound become important as the temperature is raised to near the λ point. Experimental data cited earlier in this introduction suggests that such mechanisms exist.

One possible mechanism is suggested by theoretical work[29] on the bulk liquid that resulted in the hypothesis that thermally excited vortex rings condense in the liquid at temperatures somewhat below the λ point and are responsible for an order-disorder transition at T_λ. Through the effect of the vortices on the propagation of waves, third sound could be used to investigate the validity of that hypothesis when it is extended to thick films where there is also a cusp behavior in the specific heat similar to that in bulk liquid. If the experiments are found to support the hypothesis, further third-sound experiments could be conducted to study the size and preferred orientation of those vortices.

The treatment of third-sound theory presented in this paper was initiated as part of the preflight preparations for the Superfluid Helium Experiment on NASA's Spacelab-2.[30] In addition to giving new insights into previously existing results for ground-based experiments and suggesting new paths of investigation on earth, the theory also strengthens the foundation for future basic scientific experiments in space where, in contrast to the situation on earth, films having uniform thickness in the range from tens of Å up to a few μm can be readily produced and studied.

The remainder of this paper is organized in the following way. In Sec. II the theory of third-sound propagation in thick films is developed and extended to include a heat source for excitation. Algebraic formulas for solutions of the ensuing equations are then derived. Section III contains results calculated with the aid of the newly derived formulas. Solitary waves, waves excited by long and short bursts of heat, and uniform evaporation are treated there. Both theoretical and experimental implications of the results are discussed. Section IV contains conclusions drawn from this work.

II. THEORY OF THIRD SOUND PROPAGATION IN THICK FILMS

The basic equations of third sound including a source of heat for excitation are derived in Sec. II A. This is followed by solution of those equations in Secs. II B–II D.

A. Two-fluid model with a heat source

The theory of third sound can be developed using the following dissipationless form of the two-fluid equations[31] for bulk-liquid ^{4}He.

Continuity equation:

$$\frac{\partial\rho}{\partial t}+\nabla\cdot(\rho_s\mathbf{v}_s+\rho_n\mathbf{v}_n)=0\ , \tag{1}$$

where $\rho=\rho_s+\rho_n$. The fluid mass density is ρ. The superfluid and normal fluid densities are ρ_s and ρ_n, respectively, and the corresponding velocities are $\mathbf{v}_s$ and $\mathbf{v}_n$.

Entropy conservation with a heat source:

$$\frac{\partial(\rho s)}{\partial t}+\nabla\cdot(\rho s\mathbf{v}_n)=\frac{Q}{T}\ , \tag{2}$$

where Q is the heat per unit volume injected into the liquid at a point in unit time, T is temperature, and s is entropy per unit mass.

Superfluid equation of motion with an external potential per unit mass ϕ:

$$\frac{\partial\mathbf{v}_s}{\partial t}+\mathbf{v}_s\cdot\nabla\mathbf{v}_s=-\frac{1}{\rho}\nabla p+s\nabla T+\frac{1}{2}\frac{\rho_n}{\rho}\nabla(\mathbf{v}_s-\mathbf{v}_n)^2-\nabla\phi\ , \tag{3}$$

where the superfluid, being irrotational, obeys

$$\nabla\times\mathbf{v}_s=0 \tag{4}$$

and p is the pressure.

Bergman[3,7,10] elaborated a method of deriving third-sound equations by integrating such bulk-fluid relations over the thickness of the film. That approach is formally satisfying and capable of greater precision and generality than the one we will take here. We will follow more closely Atkins'[1,2] method, which is more intuitive and more transparent. Certain simplifying assumptions in this approach restrict it to thick films. This limitation is largely due to (1) treating mass, entropy, and superfluid densities as if they take on their bulk liquid values and (2) neglecting ordinary heat conduction from the film into the substrate and vapor.

The main features of third sound can be found by considering oscillations of a film that is uniform in the z direction for the geometry shown in Fig. 1. The film is assumed to be many atomic layers thick, but the thickness is also much less than the viscous penetration depth in the normal fluid $(2\eta_n/\rho_n\omega)^{1/2}$, for all frequencies considered here. As a consequence of this second condition, the normal fluid is locked to the substrate so that to good approximation $\mathbf{v}_n=0$. The superfluid has no viscosity and moves freely, mainly parallel to the substrate. As an approximation, we will take $\mathbf{v}_s$ to be in the x direction and independent of the distance from the substrate, consistent with Eq. (4).

The liquid film is acted on by an external potential ϕ that, in general, contains contributions from gravity and from the van der Waals interaction of the helium atoms with the substrate. The van der Waals per unit mass of film is

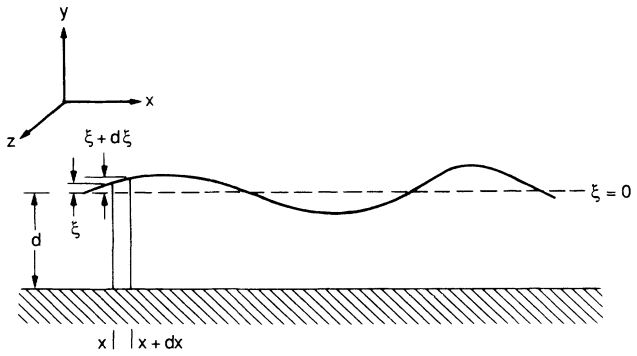

FIG. 1. Third-sound wave in a superfluid ^{4}He film.

$$\phi_W = -\frac{a}{y^3} . \tag{5}$$

The corresponding force on unit mass of the film near its outer surface is in the negative y direction and its magnitude is

$$f = \frac{3a}{d^4} , \tag{6}$$

where d is the film thickness. In the present treatment, gravity is taken into account only to the extent that it may help determine the equilibrium thickness of the film. For example, for a saturated film at height H above a liquid reservoir in a terrestrial laboratory, the film thickness is[32]

$$d = kH^{-1/3} , \tag{7}$$

where

$$k = \left[\frac{a}{g}\right]^{1/3} \simeq 4.2\times 10^{-6} \tag{8}$$

in cm$^{4/3}$ and $g = 980$ cm s^{-2}.

Turning now to the derivation of equations for third sound, refer to Fig. 1 for meanings of symbols and consider a portion of the film of width $\overline{W}$ in the z direction and lying between x and $x+dx$. For a film of thickness d, the superfluid mass crossing the face at x per unit time is $\rho_s v_s \overline{W} d$. Using Eq. (1), one finds that the net flow of the mass into the region through the faces at x and $x+dx$ is

$$\left[\frac{dM}{dt}\right]_{\text{flow}} = -\rho_s \overline{W} d \left[\frac{\partial v_s}{\partial x}\right] \delta x . \tag{9}$$

Here, and in what follows, v_s, $\partial\rho_s/\partial x$, and ξ are treated as first-order terms while terms of second order and higher are neglected.

Atkins[1,2] assumed, on the basis of kinetic theory arguments using detailed balance, that the change in mass of the liquid slab due to evaporation at its free surface is given to sufficient approximation by

$$\left[\frac{dM}{dt}\right]_{\text{evap}} = -KT'\overline{W}\delta x , \tag{10}$$

where

$$K = \gamma \left[\frac{m_{\text{He}}}{2\pi RT}\right]^{1/2} \beta . \tag{11}$$

Here γ is a constant which Atkins assumed to have the approximate value of one. Also, $\beta = dp/dT$, the derivative being evaluated on the saturated vapor-pressure curve at the unperturbed temperature T. The mass of a ^{4}He atom is m_{He}, and the gas constant per mole is R. The temperature T of the vapor at least several molecular mean free paths from the film surface is assumed to remain constant, and the instantaneous temperature of the film at x during third-sound oscillations is $T+T'$.

The net change in mass in the slab due to flow and evaporation changes the height of the surface an amount ξ, and the total mass density ρ remains constant in this approximation. Therefore,

$$\left[\frac{dM}{dt}\right]_{\text{flow}} + \left[\frac{dM}{dt}\right]_{\text{evap}} = \rho \frac{\partial \xi}{\partial t} \overline{W}\delta x . \tag{12}$$

From Eqs. (9), (10), and (12), one finds

$$\rho \left[\frac{\partial \xi}{\partial t}\right] + \rho_s d \left[\frac{\partial v_s}{\partial x}\right] + KT' = 0 . \tag{13}$$

Change of entropy in the slab of liquid is a sum of terms associated with change of mass in the slab and change in entropy density associated with temperature variations. Then,

$$\left[\frac{\partial Ms}{\partial t}\right] = s\left[\frac{dM}{dt}\right] + M\frac{\partial s}{\partial t} = s\left[\left[\frac{dM}{dt}\right]_{\text{flow}} + \left[\frac{dM}{dt}\right]_{\text{evap}}\right] + \frac{M}{T}C\frac{\partial T'}{\partial t} , \tag{14}$$

where C is the specific heat per unit mass of fluid. Superfluid flow through the faces at x and $x+dx$ does not change the entropy, as one can see by referring to Eq. (2). The entropy entering the slab is therefore just equal to a sum of two terms. One is due to condensation from the gas (negative evaporation) and is represented as $s_g(dM/dt)_{\text{evap}}$. The second is due to heat injected by a source and is represented as $q(x,t)\overline{W}\delta x$. Noting that the latent heat of vaporization is $L = T(s_g - s)$, one can combine these results with Eqs. (9), (10), and (14) and obtain, from entropy balance,

$$\rho C d\frac{\partial T'}{\partial t} - \rho_s d\frac{\partial v_s}{\partial x} sT + KLT' = q . \tag{15}$$

The final equation for third sound is found using Eq. (3). First, integrate the y component of Eq. (3) when the thickness of the film is d and the pressure is p_0, and obtain

$$p_0(x,y;T) = p_0(x,d;T) - \rho[\phi_W(y) - \phi_W(d)] . \tag{16a}$$

Next, integrate the y component of Eq. (3) when the film is perturbed by third sound; the thickness is $d+\xi$, the

temperature is $T+T'$, the pressure is p, and T' and ξ are functions of x only. Taking into account that $v_y=0$, one finds, through first-order terms,

$$p(x,y;T+T')=p(x,d+\xi;T+T') -\rho[\phi_W(y)-\phi_W(d+\xi)] . \quad (16b)$$

The variable pressure p' due to third sound is defined by

$$p(x,y;T+T')=p_0(x,y;T)+p'(x,y;T+T') . \quad (16c)$$

Combining Eqs. (16a)–(16c), one obtains

$$p'(x,y;T+T')=p(x,d+\xi;T+T')-p_0(x,d;T) +\rho[\phi_W(d+\xi)-\phi_W(d)] . \quad (16d)$$

Taylor series expansions give, through first-order terms,

$$p(x,d+\xi;T+T')=p(x,d+\xi;T)+\beta T' , \quad (16e)$$

$$\phi_W(d+\xi)=\phi_W(d)+f\xi , \quad (16f)$$

where β is the same as in Eq. (11) and where f is given by Eq. (6). If the vapor is treated[33] as an ideal gas in the presence of an external potential $\phi_W(y)$, then an elementary calculation yields

$$p(x,d+\xi;T)-p_0(x,d;T) \simeq -\rho_g(\infty)e^{-(m_{\mathrm{He}}/kT)\phi_W(d)}f\xi , \quad (16g)$$

where $\rho_g(\infty)$ is the mass density of the gas far from the substrate. Numerical evaluation of the right-hand side of Eq. (16g) shows that it is negligible for $d>100$ Å, the film thickness range in which we are interested. Taking this into account and combining Eqs. (16d)–(16g), one obtains

$$p'(x,y;T+T')=\beta T'+\rho f\xi . \quad (17)$$

Substituting Eq. (17) into (3), one finds that the x component of the linearized superfluid equation of motion is

$$\frac{\partial v_s}{\partial t}=-f\frac{\partial \xi}{\partial x}+\left[s-\frac{\beta}{\rho}\right]\frac{\partial T'}{\partial x} . \quad (18)$$

Equations (13), (15), and (18) provide the basic relations in the theory of third sound formulated by Atkins except that the heat-balance relation, Eq. (15), has been extended to include a heat source for excitation.

B. General solution of third-sound equations

A general solution of the third-sound equations will be developed here for a model of an experimental chamber shown in Fig. 2(a). Other important experimental arrangements to which our treatment can be applied with no change except proper identification of certain parameters are shown in Figs. 2(b) and 2(c). Surface disturbances excited by the localized heater shown in Fig. 2(a) travel in both directions around the annular track. A detector for thickness changes in the film is shown there as a flat comb capacitor, like that in the experimental cells that were flown on Spacelab-2.[30] However, a parallel plate capacitor with a narrow gap could serve the same purpose. Experiment[5] has shown that third sound does not propagate past steps of about 3 mm or more, and on that basis we will assume that the third sound is confined to the flat surface where the heater is located.

If the average radius of the cell is much greater than the width of the annular track, then the system with its physically imposed periodic boundary conditions can be well represented by a rectilinear model with repetitive structure extending over $-\alpha<x<\alpha$, as indicated in Fig. 3. We will consider a strip of unit width in this idealized model. The distance P is just the average of the inner and outer perimeters of the actual track. The origin of the x coordinate is chosen to be at the center of the actual heater whose length is W. The detector is located be-

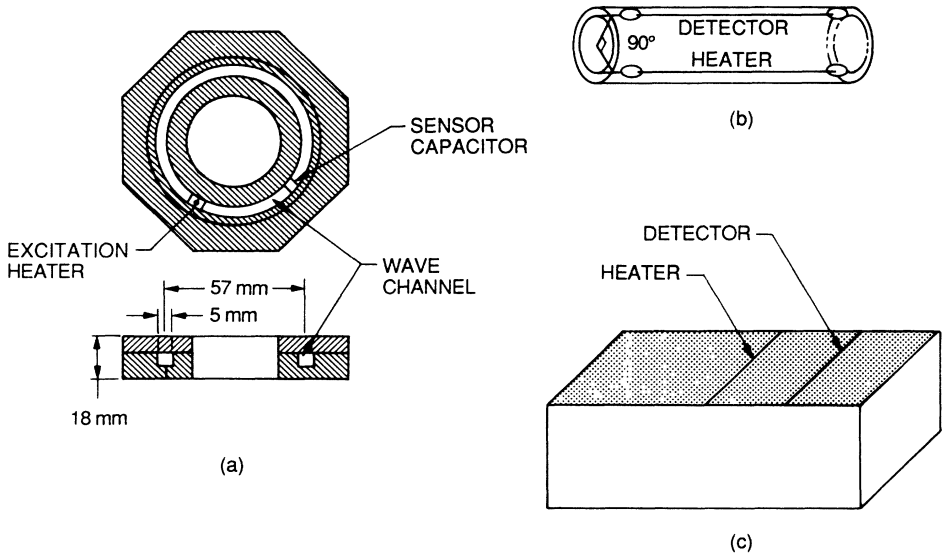

FIG. 2. Tracks for third-sound waves: (a) annular channel, (b) cylinder surface with horizontal axis, (c) horizontal flat plate.

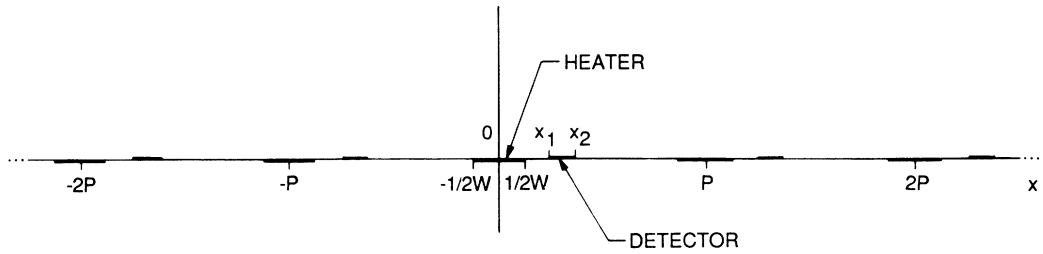

FIG. 3. Rectilinear model for third sound.

tween x_{11} and x_{12}. In the rectilinear model there are also heaters and detectors at image points implied by the periodic boundary conditions.

The heat flux density $q(x,t)$ injected into the system can be represented in terms of Fourier components $q_0(k_n,\omega)$ as follows:

$$q(x,t)=\frac{1}{P}\sum_n \int_{-\infty}^{\infty}\frac{d\omega}{2\pi}q_0(k_n,\omega)e^{i(\omega t-k_n x)}, \tag{19}$$

where $k_n=2\pi n/P$ and $n=0,\pm1,\pm2,\ldots$. This same set of one-dimensional wave vectors for the normal modes also applies to the cylinder in Fig. 2(b) and the flat plate in Fig. 2(c). In the latter case, the values of k_n are found using results for superfluid velocity developed later in this section together with the boundary conditions that $v=0$ at the edges of the actual plate, located at $x=\pm\frac{1}{2}P$. The inverse of Eq. (18) is

$$q_0(k_n,\omega)=\int_{-1/2P}^{1/2P}dx\int_{-\infty}^{\infty}dt\,q(x,t)e^{-i(\omega t-k_n x)}. \tag{20}$$

Similar equations hold for the pairs of variables $[\xi(x,t),\xi_0(k_n,\omega)]$, $[v(x,t),v_0(k_n,\omega)]$, and $[T'(x,t),T_0(k_n,\omega)]$ for surface displacement, superfluid velocity, and temperature change, respectively. The subscript is omitted from v_s here and in what follows.

Substituting Fourier representatives into the third-sound equations (13), (15), and (18) and equating coefficients of linearly independent exponentials $e^{i(\omega t-k_n x)}$, one finds the following set of simultaneous equations for the Fourier amplitudes:

$$\begin{aligned} &i\omega\rho\xi_0-ik_n\rho_s d v_0+KT_0=0,\\ &ik_n\rho_s d v_0+(i\omega\rho Cd+KL)T_0=q_0,\\ &-ik_n f\xi_0+i\omega v_0+ik_n(s-\beta/\rho)T_0=0. \end{aligned} \tag{21}$$

This system of equations can be solved using Cramer's rule. One finds

$$\xi_0=\frac{q_0\bar{N}_1}{\bar{D}},\quad v_0=\frac{q_0\bar{N}_2}{\bar{D}},\quad T_0=\frac{q_0\bar{N}_3}{\bar{D}}, \tag{22}$$

where

$$\bar{D}=\det\begin{vmatrix} i\omega\rho & -ik_n\rho_s d & K\\ 0 & ik_n\rho_s dsT & i\omega\rho Cd+KL\\ -ik_n f & i\omega & ik_n\left[s-\dfrac{\beta}{\rho}\right]\end{vmatrix}$$

$$=i\omega\rho\left[-k_n^2\rho_s d\left[s-\frac{\beta}{\rho}\right]sT\right] \tag{23a}$$

$$+(i\omega\rho Cd+KL)(-k_n^2\rho_s df)$$

$$-Kk_n^2\rho_s dfsT+\omega^2\rho(i\omega\rho Cd+KL)$$

$$\simeq\rho KL\left[\omega^2-i\frac{\rho_s dTs^2k_n^2}{KL}\omega-\frac{\rho_s df}{\rho}\left[1+\frac{Ts}{L}\right]k_n^2\right], \tag{23b}$$

$$q_0\bar{N}_1=\det\begin{vmatrix} 0 & -ik_n\rho_s d & K\\ q_0 & ik_n\rho_s dsT & i\omega\rho Cd+KL\\ 0 & i\omega & ik_n\left[s-\dfrac{\beta}{\rho}\right]\end{vmatrix}$$

$$=q_0\left[-k_n^2\rho_s d\left[s-\frac{\beta}{\rho}\right]+i\omega K\right] \tag{24a}$$

$$\simeq -q_0(\rho_s dsk_n^2-i\omega K), \tag{24b}$$

$$q_0\bar{N}_2=\det\begin{vmatrix} i\omega\rho & 0 & K\\ 0 & q_0 & i\omega\rho Cd+KL\\ -ik_n f & 0 & ik_n\left[s-\dfrac{\beta}{\rho}\right]\end{vmatrix}$$

$$=q_0\left[-\omega k_n\rho\left[s-\frac{\beta}{\rho}\right]+iKk_n f\right] \tag{25a}$$

$$\simeq q_0(-\omega k_n\rho s+iKk_n f), \tag{25b}$$

$$q_0\bar{N}_3=\det\begin{vmatrix} i\omega\rho & -ik_n\rho_s d & 0\\ 0 & ik_n\rho_s dsT & q_0\\ -ik_n f & i\omega & 0\end{vmatrix}$$

$$=q_0(-k_n^2\rho_s df+\rho\omega^2). \tag{26}$$

A factor $q_0(k_n,\omega)$ enters into the numerator of each of the Fourier amplitudes. That factor can be simplified as follows for the situation we are considering where $q(x,t)$

is spatially uniform over the face of the heater and zero elsewhere. Write the heat flux density as a product

$$q(x,t)=p(x)r(t)\ , \tag{27}$$

where

$$p(x)=\Theta(\tfrac{1}{2}W-x)\Theta(x+\tfrac{1}{2}W) \tag{28}$$

and Θ is a unit step function such that

$$\Theta(X)=\begin{cases}0 & \text{for } X<0\\ 1 & \text{for } X>0\ ,\end{cases} \tag{29}$$

Substitute Eqs. (27) and (28) into (19) and (20) and obtain

$$q_0(k_n,\omega)=\bar{P}(k_n)\bar{R}(\omega)\ , \tag{30}$$

where

$$p(x)=\frac{1}{P}\sum_n \bar{P}(k_n)e^{-ik_nx}\ , \tag{31}$$

$$\bar{P}(k_n)=\int_{-1/2P}^{1/2P}dx\,p(x)e^{ik_nx}\ , \tag{32}$$

$$r(t)=\int_{-\infty}^{\infty}\frac{d\omega}{2\pi}\bar{R}(\omega)e^{i\omega t}\ , \tag{33}$$

$$\bar{R}(\omega)=\int_{-\infty}^{\infty}dt\,r(t)e^{-i\omega t}\ . \tag{34}$$

Substituting Eqs. (22) and (30) into the analog of Eq. (19), viz,

$$\xi(x,t)=\frac{1}{P}\sum_n\int_{-\infty}^{\infty}\frac{d\omega}{2\pi}\xi_0(k_n,\omega)e^{(i\omega t-k_nx)}\ , \tag{35}$$

one finds

$$\xi(x,t)=\frac{1}{P}\sum_n\bar{P}(k_n)I_1(k_n,t)e^{-ik_nx}\ , \tag{36}$$

where, in general, for $j=1,2,3$,

$$I_j(k_n,t)=\int_{-\infty}^{\infty}\frac{d\omega}{2\pi}\bar{R}(\omega)\frac{\bar{N}_j(k_n,\omega)}{\bar{D}(k_n,\omega)}e^{i\omega t}\ . \tag{37}$$

Assuming the capacitor measures the average displacement of the liquid film from its equilibrium thickness between x_{11} and x_{12}, one finds that the detected signal is proportional to $\xi(t)$, where

$$\xi(t)=\frac{1}{x_{12}-x_{11}}\int_{x_{11}}^{x_{12}}\xi(x,t)dx\ . \tag{38}$$

This can be simplified further. Note that only even powers of k_n enter into the expressions for $\bar{D}$ and $\bar{N}_1$ in Eqs. (23) and (24). Then, with the aid of Eq. (37), one can show that $I_1(k_n,t)=I_1(-k_n,t)$. Using this result upon substituting Eq. (36) into (38) and carrying out the indicated integration, one finds the detected surface displacement is

$$\xi(t)=\frac{1}{P}\left[\bar{P}_0I_{10}(t)+\sum_{n>0}\bar{P}(k_n)I_1(k_n,t)\frac{4\sin[\frac{1}{2}k_n(x_{12}-x_{11})]\cos[\frac{1}{2}k_n(x_{12}+x_{11})]}{k_n(x_{12}-x_{11})}\right]\ . \tag{39}$$

By similar methods one can derive formulas for superfluid velocity and temperature signals when the average values are sensed by appropriate detectors. If the velocity detector is between x_{21} and x_{22}, and the temperature detector between x_{31} and x_{32}, one finds

$$\begin{aligned}v(t)&=\frac{1}{x_{22}-x_{21}}\int_{x_{21}}^{x_{22}}v(x,t)dx\\ &=\frac{1}{P}\sum_{n>0}\bar{P}(k_n)\frac{1}{i}I_2(k_n,t)\frac{4\sin[\frac{1}{2}k_n(x_{22}-x_{21})]\sin[\frac{1}{2}k_n(x_{22}+x_{21})]}{k_n(x_{22}-x_{21})}\ ,\end{aligned} \tag{40}$$

$$\begin{aligned}T'(t)&=\frac{1}{x_{32}-x_{31}}\int_{x_{31}}^{x_{32}}T'(x,t)dx\\ &=\frac{1}{P}\left[\bar{P}_0I_{30}(t)+\sum_{n>0}\bar{P}(k_n)I_3(k_n,t)\frac{4\sin[\frac{1}{2}k_n(x_{32}-x_{31})]\sin[\frac{1}{2}k_n(x_{32}+x_{31})]}{k_n(x_{32}-x_{31})}\right]\ ,\end{aligned} \tag{41}$$

where

$$\bar{P}_0\equiv\bar{P}(k_n=0)$$

and

$$I_{j0}\equiv I_j(k_n=0,t)\quad\text{for } j=1,2,3\ .$$

The terms in the right-hand sides of Eqs. (39)–(41) are separated into factors that depend on the spatial characteristics of the heater and of the detector, and on an intensity factor I_j which depends on the intrinsic properties of third-sound waves and the frequency dependence of the source. Each of these factors is a function of k_n. The terms involving $k_n=0$ were mentioned in Sec. I and seem to have been overlooked or neglected in all previous work.

The formulas for response functions $\xi(t)$, $v(t)$, and $T'(t)$ given by Eqs. (39)–(41) are exact within the context of Atkins'[1,2] theory when that theory is extended to include a heat source for excitation. Using Eqs. (28) and (32), one can show easily that when the source is centered at $x=0$, the factors $\bar{P}$ occurring there are given by

$$\bar{P}_0=W,\quad \bar{P}(k_n)=\frac{2}{k_n}\sin(\tfrac{1}{2}k_nW)\quad\text{for } k_n\neq0\ . \tag{42}$$

If the time dependence of the source is specified, then $\bar{R}(\omega)$ can be calculated and the intensity factors $I_j(k_n,t)$ in Eqs. (39)–(41) can be evaluated. The next two parts of this section are concerned with special cases where the excitation signals are simple enough to be treated analytically and complex enough to be informative and practically useful. While exact results could be obtained analytically in these cases, we will introduce certain approximations that are fairly accurate and which reduce the complexity of the mathematics considerably.

These approximations take advantage of the following inequalities, which are similar to some that Atkins[1,2] used in his work.

(1) In the range $0.6 \le T \le 2.0$ K,

$$\frac{\beta}{\rho s} < 0.07 \ .$$

(2) When $\gamma = 1$, $\omega < 10^4$ rad s^{-1} and $d < 10^{-5}$ cm,

$$C\left[\frac{KL}{\rho\omega d}\right]^{-1} < \begin{cases} 0.0060 & \text{for } 0.6 \le T \le 2.0 \text{ K} \ , \\ 0.0010 & \text{for } 0.8 \le T \le 2.0 \text{ K} \ . \end{cases}$$

These observations and neglect of small terms which can be identified with their help lead to the approximate expressions for $\bar{D}$, $\bar{N}_1$, and $\bar{N}_2$ given in Eqs. (23b), (24b), and (25b). The main benefit of using these approximate formulas stems from $\bar{D}$ being reduced from a cubic to a quadratic function of ω, as we shall see in the following two sections.

C. Excitation by rectangular heat pulses

Rectangular heat-pulse excitation signals are of interest for several reasons. One is that they can be easily generated experimentally and yet are amenable to theoretical analysis. Also, a special limiting case of this form is a Dirac δ function excitation in time, which is also useful in experimental investigations that are especially easy to analyze. Furthermore, the results obtained for rectangular pulses provide part of the solution in treating a finite burst of sine wave excitation signals, as we will see in Sec. II D.

The intensity factors $I_j(k_n,t)$ that enter formulas for $\xi(t)$, $v(t)$, and $T'(t)$ in Eqs. (39)–(41) will be evaluated next. They involve the function $\bar{R}(\omega)$ as indicated in Eq. (37). $\bar{R}(\omega)$ is the Fourier transform of $r(t)$, the time-dependent factor in the excitation signal. General properties of these functions are given in Eqs. (27), (33), and (34).

Consider first the problem of evaluating $\bar{R}(\omega)$ for a sequence of M rectangular pulses when A_m is the amplitude of the mth pulse, and $1 \le m \le M$. In the time domain, the excitation factor is

$$r(t) = \sum_m A_m \Theta(t - t_{mi}) \Theta(t_{mf} - t) \ . \tag{43a}$$

The subscripts i and f refer to initial and final instants of excitation at constant heat-flux-density input A_m. If the heat is generated by applying a voltage V_m to produce a current I_m in a resistance R having a surface area $\bar{A}$ next to the liquid-helium film, then

$$A_m = \frac{V_m^2}{R\bar{A}} \ . \tag{43b}$$

Using Eqs. (34) and (43a), one finds

$$\bar{R}(\omega) = \sum_{1 \le m \le M} i A_m \frac{1}{\omega - i\epsilon}(e^{-i\omega t_{mf}} - e^{-i\omega t_{mi}}) \ . \tag{44}$$

In Eq. (44) and throughout this paper, whenever ϵ appears in an expression that occurs somewhere in an integrand, ϵ is taken to be a positive number that tends to zero after the integral is evaluated. One can verify that the imaginary term in the denominator in Eq. (44) is correct by substituting Eq. (44) into (33) and using contour integration to show that the result is Eq. (43).

Turning now to the evaluation of the intensity factor $I_1(k_n,t)$ given by Eq. (37), one can use Eqs. (23b), (24b), and (44), then factor the function $\bar{D}(k_n,\omega)$, and obtain

$$I_1(k_n,t) = \sum_m A_m \int_{-\infty}^{\infty} \frac{d\omega}{2\pi} \frac{-D_1[\omega + i(C_1/D_1)k_n^2](e^{i\omega(t-t_{mf})} - e^{i\omega(t-t_{mi})})}{(\omega - k_n^2 E_{n+})(\omega - k_n^2 E_{n-})(\omega - i\epsilon)} \ , \tag{45}$$

where

$$A = \frac{\rho_s d T s^2}{2KL} \ , \tag{46}$$

$$B_n = \begin{cases} 0 \ \text{ for } k_n = 0 \ , \\ \dfrac{\rho_s df}{\rho k_n^2}\left[1 + \dfrac{Ts}{L}\right] \ \text{ for } k_n \neq 0 \ , \end{cases} \tag{47}$$

$$C_1 = \frac{\rho_s ds}{\rho KL} \ , \tag{48}$$

$$D_1 = \frac{1}{\rho L} \ , \tag{49}$$

$$E_{n\pm} = iA \pm (B_n - A^2)^{1/2} \ . \tag{50}$$

The integral in Eq. (45) can be readily evaluated using contour integration and the residue theorem. The major steps and results in this procedure are as follows:

$$I_1(k_n,t) = \sum_m A_m [\Theta(t - t_{mf}) S_1(k_n; t, t_{mf}) - \Theta(t - t_{mi}) S_1(k_n; t, t_{mi})] \ , \tag{51a}$$

where S_1 is defined by

$$\Theta(t-t_p)S_1(k_n;t,t_p)$$
$$=\int_{-\infty}^{\infty}\frac{d\omega}{2\pi}\frac{-D_1[\omega+i(C_1/D_1)k_n^2]e^{i\omega(t-t_p)}}{(\omega-k_n^2E_{n+})(\omega-k_n^2E_{n-})(\omega-i\epsilon)} \quad (51b)$$

and t_p represents either t_{mf} or t_{mi}. By contour integration and the residue theorem, one finds

$$S_1(k_n=0;t,t_p)=D_1(t-t_p)\ . \quad (52)$$

For $k_n\neq 0$, two cases must be considered. First, for $B_n > A^2$ one finds

$$S_1(k_n;t,t_p)\equiv S_1(k_n;t,t_p;C_1,D_1)$$
$$=-\frac{C_1}{B_nk_n^2}+\frac{1}{k_n^2}\left[\left[\frac{D_1}{(B_n-A^2)^{1/2}}+\frac{C_1A}{B_n(B_n-A^2)^{1/2}}\right]\sin[k_n^2(B_n-A^2)^{1/2}(t-t_p)]\right.$$
$$\left.+\frac{C_1}{B_n}\cos[k_n^2(B_n-A^2)^{1/2}(t-t_p)]\right]e^{-k_n^2A(t-t_p)} \quad (53a)$$
$$=-\frac{C_1}{B_nk_n^2}+\frac{1}{k_n^2}\left[\left[\frac{C_1}{B_n}\right]^2+\frac{1}{B_n-A^2}\left[D_1+\frac{C_1A}{B_n}\right]^2\right]^{1/2}$$
$$\times\sin[k_n^2(B_n-A^2)^{1/2}(t-t_p)+\phi_1]e^{-k_n^2A(t-t_p)}\ . \quad (53b)$$

The first line in the above equation indicates explicitly a dependence of S_1 on C_1 and D_1 for reasons that will become clear later. Equation (53b) exhibits the results in a particularly transparent form and is also efficient to use in numerical studies. The phase angle ϕ_1 in Eq. (53b) satisfies

$$\sin\phi_1=\frac{1}{M_1}\frac{C_1}{B_n},$$
$$\cos\phi_1=\frac{1}{M_1(B_n-A^2)^{1/2}}\left[D_1+\frac{C_1A}{B_n}\right], \quad (54a)$$

where

$$M_1=\left[\left[\frac{C_1}{B_n}\right]^2+\frac{1}{B_n-A^2}\left[D_1+\frac{C_1A}{B_n}\right]^2\right]^{1/2}. \quad (54b)$$

For $B_n < A^2$, evaluation of the integral in Eq. (51b) gives

$$S_1(k_n;t,t_p)\equiv S_1(k_n;t,t_p;C_1,D_1)$$
$$=-\frac{C_1}{B_nk_n^2}+\frac{1}{k_n^2}\left[\left[\frac{D_1}{(A^2-B_n)^{1/2}}+\frac{C_1A}{B_n(A^2-B_n)^{1/2}}\right]\sinh[k_n^2(A^2-B_n)^{1/2}(t-t_p)]\right.$$
$$\left.+\frac{C_1}{B_n}\cosh[k_n^2(A^2-B_n)^{1/2}(t-t_p)]\right]e^{-k_n^2A(t-t_p)}\ . \quad (55)$$

Using these results one can readily evaluate the response of the detector in terms of the film thickness as a function of time and position when third sound is excited by a sequence of rectangular heat pulses.

Formulas for $v(t)$ and $T'(t)$ can be found by similar methods. The results are as follows.

The intensity factor $I_2(k_n,t)$ in Eqs. (37) and (40) satisfies

$$I_2(k_n,t)=\sum_m iA_mk_n\int_{-\infty}^{\infty}\frac{d\omega}{2\pi}\frac{-D_2[\omega+i(C_2/D_2)](e^{i\omega(t-t_{mf})}-e^{i\omega(t-t_{mi})})}{(\omega-k_n^2E_{n+})(\omega-k_n^2E_{n-})(\omega-i\epsilon)} \quad (56a)$$
$$=\sum_m iA_mk_n[\Theta(t-t_{mf})S_2(k_n;t,t_{mf})-\Theta(t-t_{mi})S_2(k_n;t,t_{mi})]\ , \quad (56b)$$

where the definition of S_2 as an integral can be inferred from the above equation. Also,

$$C_2=-\frac{f}{\rho L}\ , \quad (57)$$
$$D_2=\frac{s}{KL}\ , \quad (58)$$

and for $k_n \neq 0$,

$$S_2(k_n;t,t_p) \equiv S_2(k_n;t,t_p;C_2,D_2) \tag{59a}$$

$$= S_1(k_n;t,t_p;\frac{C_2}{k_n^2},D_2) \tag{59b}$$

In words, Eqs. (59a) and (59b) state that S_2 is also given by Eqs. (53a), (53b), and (54) provided that C_1 is replaced by C_2/k_n^2 there and D_1 is replaced by D_2.

The intensity factor $I_3(k_n,t)$ in Eqs. (37) and (41) satisfies

$$I_3(k_n,t) = \sum_m A_m \int_{-\infty}^{\infty} \frac{d\omega}{2\pi} \frac{iD_3[\omega^2-(C_3/D_3)k_n^2](e^{i\omega(t-t_{mf})}-e^{i\omega(t-t_{mi})})}{(\omega-k_n^2E_{n+})(\omega-k_n^2E_{n-})(\omega-i\epsilon)} \tag{60a}$$

$$= \sum_m A_m[\Theta(t-t_{mf})S_3(k_n;t,t_{mf})-\Theta(t-t_{mi})S_3(k_n;t,t_{mi})] , \tag{60b}$$

where the definition of S_3 can be inferred from the above equations. Also

$$C_3 = \frac{\rho_s df}{\rho KL} , \tag{61}$$

$$D_3 = \frac{1}{\rho L} . \tag{62}$$

Contour integration and the residue theorem give the following results:

$$S_3(k_n=0;t,t_p) = -D_3 , \tag{63}$$

for $k_n \neq 0$ and $B_n > A^2$

$$S_3(k_n;t,t_p) = -\frac{C_3}{B_n k_n^2} + \left[\frac{A}{(B_n-A^2)^{1/2}}\left(\frac{C_3}{B_n k_n^2}+D_3\right)\sin[k_n^2(B_n-A^2)^{1/2}(t-t_p)] + \left(\frac{C_3}{B_n k_n^2}-D_3\right)\cos[k_n^2(B_n-A^2)^{1/2}(t-t_p)]\right] e^{-k_n^2 A(t-t_p)} , \tag{64}$$

for $k_n \neq 0$ and $B_n < A^2$

$$S_3(k_n;t,t_p) = -\frac{C_3}{B_n k_n^2} + \left[\frac{A}{(A^2-B_n)^{1/2}}\left(\frac{C_3}{B_n k_n^2}+D_3\right)\sinh[k_n^2(A^2-B_n)^{1/2}(t-t_p)] + \left(\frac{C_3}{B_n k_n^2}-D_3\right)\cosh[k_n^2(A^2-B_n)^{1/2}(t-t_p)]\right] e^{-k_n^2 A(t-t_p)} . \tag{65}$$

Third-sound signals generated by rectangular heat pulses can be completely characterized in terms of surface displacement, superfluid velocity, and temperature change, and those properties can be evaluated using the foregoing formulas.

D. Excitation by sinusodial bursts of electrical current

Sinusodial excitation signals are useful in studying resonance effects, and they have been used in a number of experiments reported in the literature. Formulas for third sound excited by sine waves of electrical current will be derived next.

Consider an excitation signal generated by a electrical current passing through a resistor R due to a sinusoidal burst of applied voltage V with frequency ω_0 and period $\bar{T}$. The initial and final instants in the burst are t_i and t_f, respectively. The excitation voltage is

$$V(t) = \Theta(t-t_i)\Theta(t_f-t)V_0\sin[\omega_0(t-t_i)] . \tag{66}$$

Just as in Sec. II C, we will let $\bar{A}$ be the area of one face of the resistor. Then the heat-flux density into the helium film is still given by Eq. (27), but now $r(t)$ satisfies

$$r(t) = r_A(t)+r_B(t) , \tag{67}$$

where

$$r_A(t) = \Theta(t-t_i)\Theta(t_f-t)\bar{B} , \tag{68a}$$

$$r_B(t) = -\Theta(t-t_i)\Theta(t_f-t)\bar{B}\cos[\omega_0(t-t_i)] , \tag{68b}$$

and

$$\bar{B}=\frac{1}{2}\frac{V_0^2}{R\bar{A}} . \tag{69}$$

The third-sound equations (13), (15), and (18) are linear in the quantities ξ, v, T', and q. Therefore, one can calculate the response of the film to a sum of excitations as the sum of the responses to the individual excitations. It follows that Eqs. (39)–(41) still hold provided that the intensity functions $I_j(k_n,t)$ are given by

$$I_j(k_n,t)=I_{jA}(k_n,t)+I_{jB}(k_n,t) \quad \text{for } j=1,2,3 , \tag{70}$$

where I_{jA} and I_{jB} correspond to $r_A(t)$ and $r_B(t)$, respectively. The functions $I_{jA}(k_n,t)$ are the same as those treated earlier in Sec. II C provided that one takes $M=1$ there and then sets $A_1=\bar{B}$.

The problem that remains is the evaluation of $I_{jB}(k_n,t)$. These functions are given by Eq. (37) when $\bar{R}(\omega)$ is replaced by $\bar{R}_B(\omega)$ there, and $\bar{R}_B(\omega)$ is the Fourier transform of $r_B(t)$. From Eqs. (68b), (69), and (34), one finds

$$\bar{R}_B(\omega)=\frac{\bar{B}}{2i}\left[\frac{e^{-i2\omega_0 t_i}}{\omega-2\omega_0-i\epsilon}(e^{i(2\omega_0-\omega)t_f}-e^{i(2\omega_0-\omega)t_i})+\frac{e^{i2\omega_0 t_i}}{\omega+2\omega_0-i\epsilon}(e^{-i(2\omega_0+\omega)t_f}-e^{-i(2\omega_0+\omega)t_i})\right] . \tag{71}$$

One can verify that the imaginary terms in the denominators are correct by substituting Eq. (71) into the right-hand side of Eq. (34), using contour integration and the residue theorem, and showing that the result is the same as the right-hand side in Eq. (68b).

Substituting Eq. (71) into (37), one can evaluate the integral by a straightforward but lengthy procedure using contour integration. Some of the major steps and results will be given here.

For $j=1$, it is useful to introduce an auxiliary function W_1 as follows:

$$\Theta(t-t_p)W_1(k_n;t,t_p;\omega_a)=\Theta(t-t_p)W_1(k_n;t,t_p;\omega_a;C_1,D_1)$$
$$\equiv\int_{-\infty}^{\infty}\frac{d\omega}{2\pi}\frac{D_1[\omega+i(C_1/D_1)k_n^2]e^{i\omega(t-t_p)}}{(\omega-k_n^2E_{n+})(\omega-k_n^2E_{n-})(\omega-\omega_a-i\epsilon)} . \tag{72}$$

Integration yields the following results:

$$I_{1B}(k_n,t)=\bar{B}\{\Theta(t-t_f)\mathrm{Re}[W_1(k_n;t,t_f;2\omega_0)e^{i2\omega_0(t_f-t_i)}]-\Theta(t-t_i)\mathrm{Re}W_1(k_n;t,t_i;2\omega_0)\} . \tag{73}$$

For $k_n=0$,

$$\mathrm{Re}[W_1(k_n;t,t_f;2\omega_0)e^{i2\omega_0(t_f-t_i)}]=\frac{\bar{B}D_1}{2\omega_0}\{\sin[2\omega_0(t_f-t_i)]-\sin[2\omega_0(t-t_i)]\} . \tag{74}$$

The second term in Eq. (73) can be evaluated by setting $t_f=t_i$ in Eq. (74). The result is

$$\mathrm{Re}W_1(k_n;t,t_i;2\omega_0)=-\frac{\bar{B}D_1}{2\omega_0}\sin[2\omega_0(t-t_i)] . \tag{75}$$

Combining these results, one obtains

$$I_{1B}(k_n=0,t)=\begin{cases}0, & t<t_i,\\ \dfrac{\bar{B}D_1}{2\omega_0}\sin[2\omega_0(t-t_i)], & t_i<t<t_f,\\ \dfrac{\bar{B}D_1}{2\omega_0}\sin[2\omega_0(t-t_i)], & t>t_f .\end{cases} \tag{76}$$

For $k_n\neq 0$, one must consider the cases $B_n>A^2$ and $B_n<A^2$ separately. For $B_n>A^2$:

$$\mathrm{Re}[W_1(k_n;t,t_f;2\omega_0)e^{i2\omega_0(t_f-t_i)}]=D_1\left[\frac{1}{2\omega_n}\left[-\sin(\omega_n t+\phi_1)-\sin(\omega_n t-\phi_2)+\frac{M_3}{M_4}\cos(\omega_n t+\phi_1+\phi_3-\phi_4)+\frac{M_3}{M_5}\cos(\omega_n t-\phi_2-\phi_3+\phi_5)\right]e^{-k_n^2A(t-t_f)}-\frac{M_3}{k_n^2M_4M_5}\cos[2\omega_0(t-t_i)+\phi_3-\phi_4-\phi_5]\right] , \tag{77}$$

where

$$\omega_n \equiv k_n^2 (B_n - A^2)^{1/2} , \tag{78}$$

$$\phi_1 \equiv (2\omega_0 - \omega_n) t_f - 2\omega_0 t_i , \tag{79}$$

$$\phi_2 \equiv (2\omega_0 + \omega_n) t_f - 2\omega_0 t_i , \tag{80}$$

$$\sin\phi_3 = \frac{2\omega_0}{k_n^2 M_3}, \quad \cos\phi_3 = -\frac{C_1}{D_1 M_3} \tag{81}$$

with

$$M_3 = \left[\left[\frac{C_1}{D_1} \right]^2 + \left[\frac{2\omega_0}{k_n^2} \right]^2 \right]^{1/2} , \tag{82}$$

$$\sin\phi_4 = \frac{A}{M_4}, \quad \cos\phi_4 = \frac{\omega_n - 2\omega_0}{k_n^2 M_4} \tag{83}$$

with

$$M_4 = \frac{1}{k_n^4} [(\omega_n - 2\omega_0)^2 + A^2]^{1/2} , \tag{84}$$

$$\sin\phi_5 = -\frac{A}{M_5}$$

and

$$\frac{3\pi}{2} \le \phi_5 \le 2\pi \tag{85}$$

with

$$M_5 = \left[\frac{1}{k_n^4} (\omega_n + 2\omega_0)^2 + A^2 \right]^{1/2} . \tag{86}$$

The second term in Eq. (73) can be evaluated by setting $t_f = t_i$ in Eqs. (77)–(81). The results are as follows:

$$\begin{aligned} \mathrm{Re} W_1(k_n;t,t_i;2\omega_0) = D_1 \Bigg[\frac{1}{2\omega_n} \Bigg[& -\sin(\omega_n t + \bar{\phi}_1) - \sin(\omega_n t - \bar{\phi}_2) + \frac{M_3}{M_4} \cos(\omega_n t + \bar{\phi}_1 + \phi_3 - \phi_4) \\ & + \frac{M_3}{M_5} \cos(\omega_n t - \bar{\phi}_2 - \phi_3 + \phi_5) \Bigg] e^{-k_n^2 A (t - t_i)} \\ & - \frac{M_3}{k_n^2 M_4 M_5} \cos[2\omega_0 (t - t_i) + \phi_3 - \phi_4 - \phi_5] \Bigg] , \end{aligned} \tag{87}$$

where

$$\bar{\phi}_1 = -\bar{\phi}_2 = -\omega_n t_i . \tag{88}$$

Notice that for all times $t > t_f$ the undamped terms that enter the expression $I_{1B}(k_n,t)$, Eq. (73), through its dependence on Eqs. (77) and (87) cancel each other. Therefore, for all $t > t_f$, the contributions of each normal mode to the intensity functions $I_{1A}(k_n,t)$ and $I_{1B}(k_n,t)$ are exponentially damped in time. Although we have seen this only for $B_n < A^2$, one can readily establish this for $B_n > A^2$ also, as well as for $I_2(k_n,t)$ and $I_3(k_n,t)$.

For $B_n < A^2$:

$$\begin{aligned} \mathrm{Re}[W_1(k_n;t,t_f;2\omega_0) e^{i2\omega_0(t_f - t_i)}] = \frac{D_1}{2k_n^2 (A^2 - B_n)^{1/2}} \Bigg[& -2\sinh[k_n^2 (A^2 - B_n)^{1/2} (t - t_f)] \cos[2\omega_0 (t_f - t_i)] \\ & - \frac{M_6}{M_7} e^{-k_n^2 (A^2 - B_n)^{1/2} (t - t_f)} \cos[2\omega_0 (t_f - t_i) + \phi_6 - \phi_7] \\ & + \frac{M_6}{M_8} e^{k_n^2 (A^2 - B_n)^{1/2} (t - t_f)} \cos[2\omega_0 (t_f - t_i) + \phi_6 - \phi_8] \Bigg] e^{-k_n^2 A (t - t_f)} \\ & - \frac{D_1 M_6}{k_n^2 M_7 M_8} \sin[2\omega_0 (t - t_i) + \phi_6 - \phi_7 - \phi_8] , \end{aligned}$$

where

$$\sin\phi_6 = \frac{C_1}{D_1 M_6}, \quad \cos\phi_6 = \frac{2\omega_0}{k_n^2 M_6} \tag{90}$$

with

$$M_6 = \left[\left[\frac{C_1}{D_1} \right]^2 + \left[\frac{2\omega_0}{k_n^2} \right]^2 \right]^{1/2} , \tag{91}$$

$$\cos\phi_7 = \frac{2\omega_0}{k_n^2 M_7} \tag{92}$$

and

$$\frac{3\pi}{2} \leq \phi_7 \leq 2\pi$$

with

$$M_7 = \left[\left(\frac{2\omega_0}{k_n^2} \right)^2 + [A + (A^2 - B_n)^{1/2}]^2 \right]^{1/2}, \tag{93}$$

$$\cos\phi_8 = \frac{2\omega_0}{k_n^2 M_8}$$

and (94)

$$\frac{3\pi}{2} \leq \phi_8 \leq 2\pi$$

with

$$M_8 = \left[\left(\frac{2\omega_0}{k_n^2} \right)^2 + [A - (A^2 - B_n)^{1/2}]^2 \right]^{1/2}. \tag{95}$$

Setting $t_f = t_i$ in Eq. (89), one finds that the second term in the right-hand side of Eq. (73) is given by

$$\begin{aligned} \mathrm{Re} W_1(k_n;t,t_i;2\omega_0) = {} & \frac{D_1}{2k_n^2 (A^2 - B_n)^{1/2}} \\ & \times \left[-2\sinh[k_n^2 (A^2 - B_n)^{1/2}(t - t_i)] - \frac{M_6}{M_7} e^{-k_n^2 (A^2 - B_n)^{1/2}(t - t_i)} \cos(\phi_6 - \phi_7) \right. \\ & \left. + \frac{M_6}{M_8} e^{k_n^2 (A^2 - B_n)^{1/2}(t - t_i)} \cos(\phi_6 - \phi_8) \right] e^{-k_n^2 A (t - t_i)} \\ & - \frac{D_1 M_6}{k_n^2 M_7 M_8} \sin[2\omega_0 (t - t_i) + \phi_6 - \phi_7 - \phi_8] . \end{aligned} \tag{96}$$

Turning next to the velocity response function, we will consider $I_2(k_n,t)$ in Eq. (37) when $\bar{R}(\omega)$, $\bar{N}_2(k_n,\omega)$, and $\bar{D}(k_n,\omega)$ are given by Eqs. (71), (25b) and (23b), respectively. In this instance, it is convenient to introduce a function W_2 as follows:

$$\begin{aligned} \Theta(t - t_p) W_2(k_n;t,t_p;\omega_a) &= \Theta(t - t_p) W_2(k_n;t,t_p;\omega_a;C_2,D_2) \\ &\equiv \int_{-\infty}^{\infty} \frac{d\omega}{2\pi} \frac{D_2[\omega + i(C_2/D_2)] k_n^2 e^{i\omega(t - t_p)}}{(\omega - k_n^2 E_{n+})(\omega - k_n^2 E_{n-})(\omega - \omega_a - i\epsilon)} , \end{aligned} \tag{97}$$

where C_2 and D_2 are given by Eqs. (57) and (58), respectively.

Using Eqs. (24b), (25b), (37), (72), (73), and (97), one can show that

$$I_{2B}(k_n,t) = ik_n \bar{B} \{ \Theta(t - t_f) \mathrm{Re}[W_2(k_n;t,t_f;2\omega_0;C_2,D_2) e^{i2\omega_0 (t_f - t_i)}] - \Theta(t - t_i) \mathrm{Re} W_2(k_n;t,t_i;2\omega_0;C_2,D_2) \} , \tag{98}$$

where, for $k_n \neq 0$,

$$W_2(k_n;t,t_p;2\omega_0;C_2,D_2) = W_1(k_n;t,t_p;2\omega_0;C_2/k_n^2,D_2) . \tag{99}$$

The function W_1 above is defined by Eq. (72) and it satisfies Eqs. (77) and (87) for $B_n > A^2$. It satisfies Eqs. (89) and (96) for $B_n < A^2$. Combining these results with Eq. (40), one can evaluate the contribution to the velocity response function $v(t)$ associated with $r_B(t)$.

Finally, we will consider the temperature-response function for a sinusoidal burst of excitation current. Referring to Eq. (70), we will evaluate $I_{3B}(k_n,t)$, which corresponds to the excitation function $r_B(t)$. The result for I_{3B} can be substituted into Eq. (41) to evaluate $T'(t)$.

The intensity function I_{3B} is given by Eq. (37) when $\bar{R}(\omega)$, $\bar{N}_3(k_n,\omega)$, and $\bar{D}(k_n,\omega)$ are given by Eqs. (71), (26), and (23b), respectively. Now it is useful to introduce a function W_3 as follows:

$$\Theta(t - t_p) W_3(k_n;t,t_p;\omega_a) \equiv \int_{-\infty}^{\infty} \frac{d\omega}{2\pi} \frac{-iD_3[\omega^2 - (C_3/D_3)k_n^2] e^{i\omega(t - t_p)}}{(\omega - k_n^2 E_{n+})(\omega - k_n^2 E_{n-})(\omega - \omega_a - i\epsilon)} . \tag{100}$$

Applying the methods used earlier, one finds

$$I_{3B}(k_n,t)=\bar{B}\{\Theta(t-t_f)\mathrm{Re}[W_3(k_n;t,t_f;2\omega_0)e^{i2\omega_0(t_f-t_i)}]-\Theta(t-t_i)\mathrm{Re}W_3(k_n;t,t_i;2\omega_0)\}\ . \tag{101}$$

The derivation of Eq. (101) uses the condition that

$$W_3^*(k_n;t,t_p;\omega_a)=W_3(k_n;t,t_p;-\omega_a)\ , \tag{102}$$

where the asterisk means complex conjugation. The validity of Eq. (102) can be established from formulas for W_3 obtained from Eq. (100) using contour integration and the residue theorem. That procedure also yields the following results:

$$W_3(k_n=0;t,t_p;\omega_a)=D_3e^{i\omega_a(t-t_p)}\ . \tag{103}$$

From Eqs. (101) and (103), one finds

$$I_{3B}(k_n=0,t)=\bar{B}D_3\{\Theta(t-t_f)\cos[2\omega_0(t-t_i)]-\Theta(t-t_i)\cos[2\omega_0(t-t_i)]\} \tag{104a}$$

$$=\begin{cases}0, & t<t_i,\\ -\bar{B}D_3\cos[2\omega_0(t-t_i)], & t_i<t<t_f\ ,\\ 0, & t>t_f\ .\end{cases} \tag{104b}$$

For $k_n\neq 0$, one must consider separately the cases where $B_n>A^2$ and $B_n<A^2$. The results are as follows.

For $B_n>A^2$:

$$\mathrm{Re}[W_3(k_n;t,t_f;2\omega_0)e^{i2\omega_0(t_f-t_i)}]=D_3\left\{\left[\frac{k_n^2B_n}{2\omega_nM_4}\cos(\omega_nt+\phi_1+2\phi_9-\phi_4)+\frac{k_n^2B_n}{2\omega_nM_5}\cos(\omega_nt-\phi_2+2\phi_9+\phi_5)\right.\right.$$
$$\left.-\frac{C_3}{2\omega_nD_3}\left[\frac{1}{M_4}\cos(\omega_nt+\phi_1-\phi_4)+\frac{1}{M_5}\cos(\omega_nt-\phi_2+\phi_5)\right]\right]e^{-k_n^2A(t-t_f)}$$
$$\left.-\frac{(4\omega_{n0}^2/k_n^2)-(C_3/D_3)}{k_n^2M_4M_5}\cos[2\omega_0(t-t_i)-\phi_4-\phi_5]\right\}\ , \tag{105}$$

where

$$\sin\phi_9=\frac{A}{B_n^{1/2}} \tag{106}$$

and

$$0\le\phi_9\le\frac{\pi}{2}\ .$$

The second term in Eq. (101) can be evaluated by setting $t_f=t_i$ in Eq. (105). The results are as follows:

$$\bar{R}eW_3(k_n;t,t_i;2\omega_0)=D_3\left\{\left[\frac{k_n^2B_n}{2\omega_nM_4}\cos(\omega_nt+\bar{\phi}_1+2\phi_9-\phi_4)+\frac{k_n^2B_n}{2\omega_nM_5}\cos(\omega_nt-\bar{\phi}_2+2\phi_9+\phi_5)\right.\right.$$
$$\left.-\frac{C_3}{2\omega_nD_3}\left[\frac{1}{M_4}\cos(\omega_nt+\bar{\phi}_1-\phi_4)+\frac{1}{M_5}\cos(\omega_nt-\bar{\phi}_2+\phi_5)\right]\right]e^{-k_n^2A(t-t_i)}$$
$$\left.-\frac{(4\omega_{n0}^2/k_n^2)-(C_3/D_3)}{k_n^2M_4M_5}\cos[2\omega_0(t-t_i)-\phi_4-\phi_5]\right\}\ . \tag{107}$$

For $B_n<A^2$:

$$\mathrm{Re}[W_3(k_n;t,t_f;2\omega_0)e^{i2\omega_0(t_f-t_i)}]=D_3\left\{\left[\left[\frac{k_n^2[A+(A^2-B_n)^{1/2}]^2+C_3/D_3}{2k_n^2(A^2-B_n)^{1/2}M_7}\right]e^{-k_n^2(A^2-B_n)^{1/2}(t-t_f)}\sin[2\omega_0(t_f-t_i)-\phi_7]\right.\right.$$
$$-\left[\frac{k_n^2[A-(A^2-B_n)^{1/2}]^2+C_3/D_3}{2k_n^2(A^2-B_n)^{1/2}M_8}\right]e^{k_n^2(A^2-B_n)^{1/2}(t-t_f)}$$
$$\left.\times\sin[2\omega_0(t_f-t_i)-\phi_8]\right]e^{-k_n^2A(t-t_i)}$$
$$\left.+\frac{[(2\omega_0/k_n)^2-C_3/D_3]}{k_n^2M_7M_8}\cos[2\omega_0(t-t_i)-\phi_7-\phi_8]\right\}. \tag{108}$$

The second term in Eq. (101) can now be evaluated by setting $t_f=t_i$ in Eq. (108). The results are as follows:

$$\mathrm{Re}W_3(k_n;t,t_i;2\omega_0)=D_3\left\{\left[-\left[\frac{k_n^2[A+(A^2-B_n)^{1/2}]^2+C_3/D_3}{2k_n^2(A^2-B_n)^{1/2}M_7}\right]e^{-k_n^2(A^2-B_n)^{1/2}(t-t_i)}\sin\phi_7\right.\right.$$
$$+\left[\frac{k_n^2[A-(A^2-B_n)^{1/2}]^2+C_3/D_3}{2k_n^2(A^2-B_n)^{1/2}M_8}\right]e^{k_n^2(A^2-B_n)^{1/2}(t-t_i)}\sin\phi_8\left.\right]e^{-k_n^2A(t-t_i)}$$
$$\left.+\frac{[(2\omega_0/k_n)^2-C_3/D_3]}{k_n^2M_7M_8}\cos[2\omega_0(t-t_i)-\phi_7-\phi_8]\right\}. \tag{109}$$

When these results for W_3 are substituted into Eq. (101) and then combined with Eq. (41), the temperature response function $T'(t)$ will be expressed as an algebraic formula.

Some features of the response functions that have important implications for experiments are revealed by the formulas that we have derived. For clarity we will describe them in terms of the displacement response function $\xi(t)$, but there are analogous features in the response functions for superfluid velocity and temperature change also.

First, there is no true steady-state condition for third sound produced by the kinds of excitations that we have analyzed. While the heater is energized, there is a net evaporation of the film that reduces the average film thickness. This net evaporation is associated with the $k_n=0$ terms in Eqs. (52) and (74). After the heater is turned off, the third-sound amplitude associated with *each resonance* decays exponentially at a characteristic rate, as indicated by Eqs. (53b) and (55) for rectangular excitation pulses and by those same two equations together with Eqs. (77), (87), (89), and (99) for sinusoidal excitation. Second, if sinusoidal excitation is applied for a long time interval, terms in the response function that decay exponentially will eventually be negligible. Then the response of the detector will be dominated by the $k_n=0$ terms together with the last terms in the right-hand sides of Eqs. (87) and (96), which oscillate at the driving frequency of the heater power. The factor M_4 in the denominator of the last term of Eq. (87) determines the line shape of the response function near each resonance. The formula for M_4 given by Eq. (84) shows how the width of the line for a resonance is related to the time decay of a normal mode.

An approximate expression for the phase velocity c of third sound found by Atkins,[12] viz,

$$c=\frac{\omega}{k}=\left[\frac{\rho_s}{\rho}df\left[1+\frac{Ts}{L}\right]\right]^{1/2},$$

can be obtained by using Eqs. (47) and (78) for the nth normal mode and taking $A=0$, which is valid when third-sound attenuation is negligible.

The formulas developed in this section provide a complete set of relations for characterizing third-sound waves excited by a sequence of rectangular pulses and by a sinusoidal burst of heat. In the next section they will be used in a numerical study of a number of cases that are of interest both theoretically and experimentally.

III. CALCULATED RESULTS

Formulas derived in Sec. II have been applied in calculating third-sound characteristics for a number of experimental configurations and a variety of excitation signals. Results will be presented for solitary waves, waves excited by long and short bursts of heat, and for uniform evaporation. Both the theoretical and experimental significance of the results will be discussed.

A. Solitary waves

Solitary waves of third sound are isolated ripples that propagate on the surface of ^{4}He films following excitation by heat pulses of very short duration at a narrow source. Existence of these waves is one of the striking predictions of the new theoretical calculations. They have not yet been observed experimentally. Solitary waves are especially well suited to elucidation of the nature of third sound in terms of correlations among a complete set of variables that characterize the dynamics of ^{4}He films, viz., surface displacement, temperature change, and velocity of superfluid parallel to the substrate. The study of

these relationships clearly shows that earlier explanations of the structure of third sound are not correct, and the actual structure of solitary waves is displayed graphically. Furthermore, the calculations reveal, for the first time, how third-sound waves are generated at a heater.

Intrinsic shapes of solitary waves in space and time domains are determined by properties of the film alone. These shapes can be found by progressively reducing the duration of the exciting heat pulse and the lengths of the heater and detector until wave forms are reached that are independent of those parameters.

Solitary waves can be generated only on films in a certain thickness range. Our calculations show that, at 1.80 K, they can exist on films at least as thin as 300 Å and at least as thick as 1000 Å. For the range of parameters we have studied numerically, they cannot be excited on films as thick as 3000 Å.

The calculations in Sec. III A are for third sound on an annular track as depicted in Fig. 2(a); the average circumference is $P=17.94$ cm. The unperturbed temperature is 1.80 K. The thickness of the film is 300 Å, and the lengths of the heater and detector along the paths of the waves are 0.01 and 0.04 cm, respectively, unless stated otherwise. The excitation starts at $t=0$ and lasts for 100 μs. These parameters satisfy the criteria described earlier for observing intrinsic properties of solitary waves.

The value of the coefficient γ is taken as 1.0 for these illustrative calculations. The properties of main interest in Sec. III A, with the exception of the attenuation, do not depend sensitively on this value. The question of determining the correct value of γ will be addressed in Sec. III D.

All curves calculated in Sec. III A take into account the normal modes $n=0-400$, unless it is explicitly stated to be otherwise. Parametric studies showed that this is adequate to avoid spurious features that were sometimes prominent when fewer normal modes, even as many as 100, were taken into account. Some characteristics of normal modes under the conditions stated above are given in Table I. The phase velocity $c=\omega k^{-1}$ varies about 0.01% for the modes $n=1-400$, and equals 76.51 cm s^{-1}. The group velocity $u=d\omega/dk$ is essentially equal to the phase velocity in this case. The decay time of a normal mode is $\tau=1/(Ak^2)$, where A is given by Eq. (46). For the conditions assumed here, $A=8.546\times10^{-3}$ cm^2 s^{-1}. The period is $\bar{T}=2\pi/\omega$.

Responses of detectors located one-quarter of the distance around the track, i.e., centered at $x=4.486$ cm, are shown in Figs. 4(a)–4(c). For detectors such as these, which are far from the source, the detected waveforms are independent of the shapes of the excitation pulses provided that the pulses are of sufficiently short duration. From Fig. 4(a) one can see that a solitary wave is a depression in the surface of the film that propagates at the common phase velocity of the normal modes. The detected signal lasts about 0.025 s, which is several times greater than the time of flight of a point with a constant phase in the wave, for example, the point of maximum depression, across a span equal to the sum of the lengths of the heater and detector. From Fig. 4(b) one can see that the temperature of the film at the detector first rises above the unperturbed level and then falls below it as the pulse moves past. The temperature change is proportional to the negative *time derivative* of the surface displacement. Figure 4(c) shows that at the location of this detector the superfluid velocity is directed toward the source, opposite to the direction of propagation of the wave, at every instant. The magnitude of that velocity is proportional to the displacement of the surface.

The properties of solitary waves are displayed as snapshots in Figs. 5(a)–5(c), where the entire track is viewed at a given instant, viz., $t=0.0585$ s. At this time, the maximum depression of the film is over the centers of the detectors specified for the previous figures. Now one can see the two waves that travel in opposite directions around the track.

These figures show that, at a given instant, the temperature change of the film is proportional to the *spatial derivative* of the surface displacement, and that the magnitude of the superfluid velocity is proportional to the surface displacement itself. Throughout the spatial extent of the solitary wave, the superfluid velocity is directed toward the heater where the pulse originated. The results in Figs. 4 and 5 are consistent with the picture that the signals in Figs. 4(a)–4(c) are generated when the wave forms in Fig. 5 move across the fixed detector at the common phase velocity of the normal modes, as one expects for a traveling wave when damping is small.

The temperature distribution is such that there is a net evaporation of liquid at any fixed point on the track that is on the leading edge of the surface depression. There is a net condensation at any point on the trailing edge. This distillation process contributes to the propagation of the depression away from the source. Furthermore, the nonuniformity of the superfluid velocity is such that, during any small time internal δt, there is a net decrease of mass in any fixed strip δx on the leading edge of the depression and a net increase on the trailing edge, as one can see with the aid of the continuity equation and Figs. 5(a) and 5(c). The resulting changes in the height of the film are about an order of magnitude greater for uneven liquid flow than for distillation over most of the solitary

TABLE I. Calculated properties of normal modes for conditions specified in text with $P=17.94$ cm.

N	k (cm^{-1})	ω (rad s^{-1})	$\bar{T}$ (s)	τ (s)	c (cm s^{-1})
1	0.350 233	26.7983	0.234 462	920.689	76.5156
2	0.700 467	53.5966	0.117 231	230.172	76.5155
100	35.023 3	2 679.81	$0.234\,464\times10^{-2}$	$0.920\,689\times10^{-1}$	76.5151
400	140.093	10 718.0	$0.586\,228\times10^{-3}$	$0.575\,431\times10^{-2}$	76.5063

wave, and further analysis shows that this is true for any value of γ. Further calculations show that, for this example where $\gamma=1.0$, over most of the wave the hydrostatic pressure is about 100 times more effective than the fountain pressure in accelerating the superfluid. It should be noted, however, that if one assumed $\gamma=0.01$, these pressures would be of comparable effectiveness.

These calculated results disagree with earlier explanations[1,2] of the structure of third sound. Atkins[1] assumed that "$\cdots$ at a peak of a wave an excess of superfluid has collected and the temperature at this point is lowered, while at a trough the temperature is raised, so that in addition to the pressure gradient present in the case of a classical liquid there is an additional restoring force due to the thermomechanical effect of the temperature gradient. Also at the trough where the film is hot it will evaporate into the vapor phase, whereas at the peak the vapor will condense on to the film. There will be a flow of vapor from the troughs to the peaks, $\cdots$." The initial assumption that troughs will be at higher temperatures is in conflict with calculated results in Figs. 5(a) and 5(b). Therefore, distillation and the thermomechanical effect do not act to produce motion of the film in the manner predicted by Atkins. This conflict was found for all solitary waves as well as all other third-sound waves that we have analyzed. Also, it can be shown that Atkins' picture does not apply for any individual normal mode. (Atkins derived formulas that indicate the correct phase relations among oscillating variables in the case of individual plane waves, which are simply related to normal modes [see Eqs. (17) and (18) of Ref. 1]. Those relations were not incorporated properly in Atkins' explanation (Ref. 1) of the structure of third sound in thick films, and the resulting error has propagated through the literature.) It may be noteworthy that the manner in which the three primary variables are correlated is simpler in solitary waves than in many of the other third-sound waves we have examined, and therefore analysis of their structure is particularly instructive.

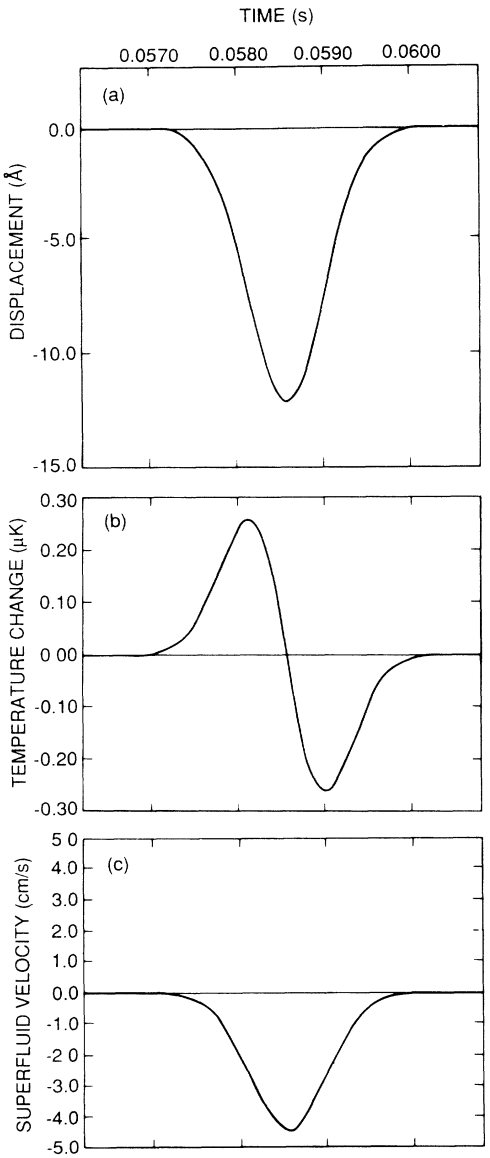

FIG. 4. Solitary waves on an annular track at a fixed detector located one-quarter of the track length from the heater: (a) surface displacement vs time, (b) temperature change vs time, (c) superfluid velocity vs time.

The process of creation of a solitary wave at a heater can be understood with the aid of Figs. 6(a)–6(c). In this example, the excitation signal is a sine wave of voltage $V_0\sin\omega_0 t$, so that the input power at the heater is proportional to $\frac{1}{2}V_0^2(1-\cos 2\omega_0 t)$. The heater was assumed to be energized for one full period of the cosine term, which was taken as 10 μ s. Also, the heater and detectors were taken to coincide in the calculations for Figs. 6(a) and 6(b), their common length along the track being 0.01 cm. Figure 6(a) shows that the thickness of the film over the heater decreases monotonically while the heater is energized, creating a trough in the surface of the film. Figure 6(b) shows that the temperature tracks the input power as a function of time, first rising above the unperturbed value and then falling, reaching the unperturbed temperature when the input power is reduced to zero. The average superfluid velocity is zero across the heater, as one can deduce from a symmetry argument. Therefore, this function is not plotted here. Instead, the superfluid velocity over a hypothetical 10-Å wide sensor placed at the edge of the heater on the positive x axis is shown in Fig. 6(c), where one can see that the velocity there is always directed toward the heater and that its magnitude increases monotonically while the heater is energized. The mass fluxes due to distillation and liquid flow into the region over the heater have been calculated using the data in those figures. The results show that evaporation is the dominant process in changing the liquid mass there.

From the foregoing discussion, one can see that a solitary wave of third sound is created at the heater by formation of a depression in the liquid-film surface, mainly due to evaporation. The liquid adjacent to the film then flows in such a way as to fill that trough, and a ripple propagates as each element of the film creates a depression that is subsequently filled by liquid flowing from the neighboring region down the line, aided to a small degree by distillation.

In contrast to solitary waves on a 300-Å thick film just discussed, solitary waves on a 1000-Å thick film undergo substantial attenuation when they propagate. This is illustrated in Fig. 7. The length of the detector was taken as 0.4 cm in that example, rather than the 0.04 cm used previously, but the other conditions were the same as specified earlier. Flight time accounts for about 30% of the width of the pulse in this case. In this instance the attenuation of the pulse is not a consequence of wave-packet spreading due to dispersion. In fact, the phase velocity, about 12.55 $\mathrm{cm\,s^{-1}}$, varies by only 0.3% for the normal modes of $n=1-100$, which give an accurate representation of the surface displacement in this particular case. A study of those 100 dominant modes shows that the attenuation and spreading of the solitary wave is due to the differing decay rates of those modes. We are not aware of this interesting decay mechanism being identified in any prior theoretical discussion of wave phenomena, although it is consistent with the certain results obtained from experiments by Generazio and Reed.[13]

Under the same conditions assumed for Fig. 7 with the single exception that the unperturbed film thickness is 3000 Å, the third-sound signal generated is no longer a solitary wave, but rather a complex wave shown in Fig. 8. Only the modes $n=1-78$ were propagating sinusoidally in this case, and only even-numbered modes could be sensed by the film-thickness detector centered at the 90° point on the annular track. A study of the properties of

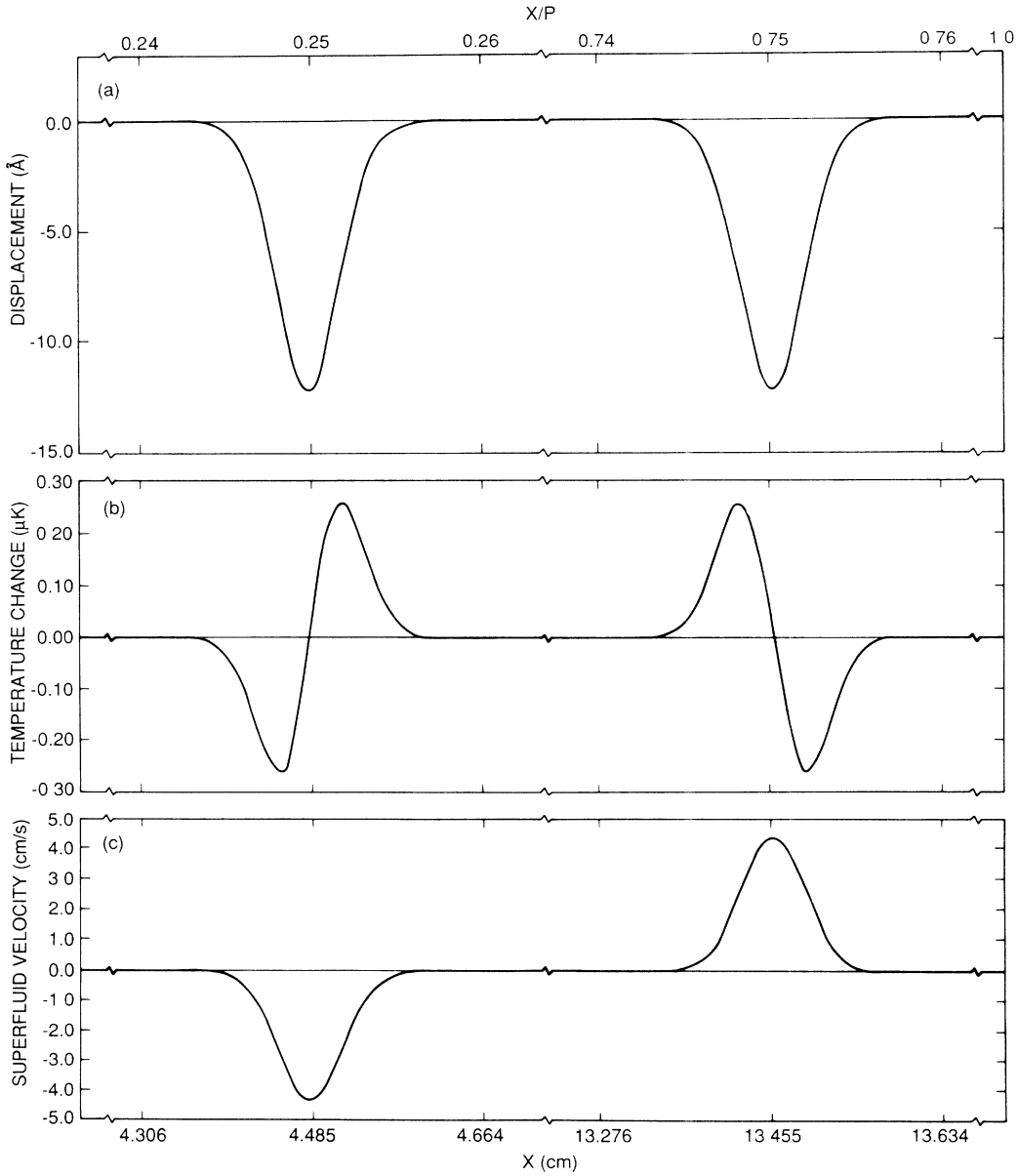

FIG. 5. "Snapshot" of solitary waves on an annular track at a fixed instant of time 0.0585 s after the heater is first excited: (a) surface displacement vs distance, (b) temperature change vs distance, (c) superfluid velocity vs distance.

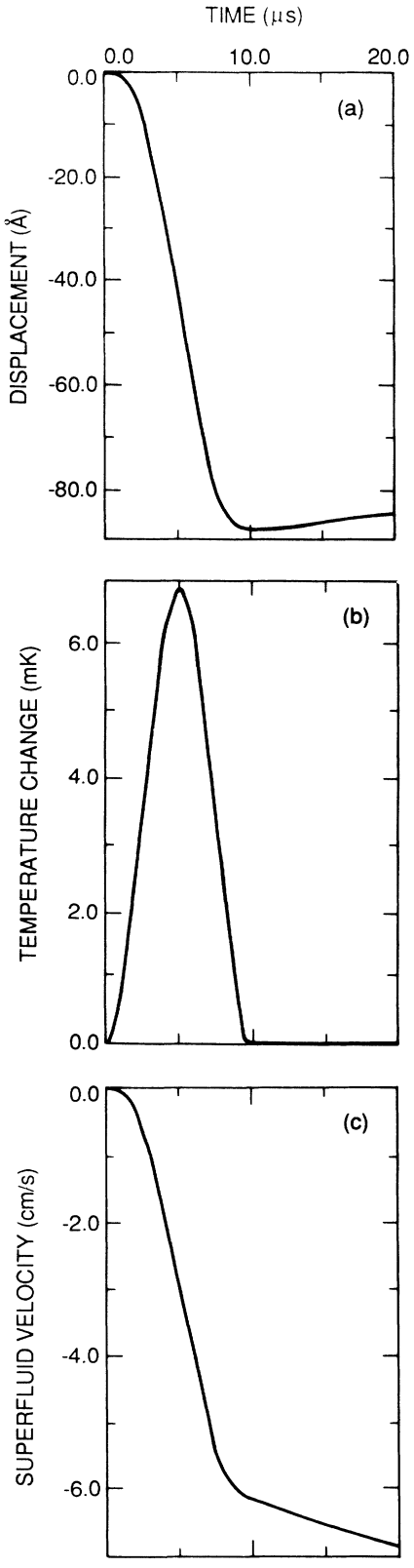

FIG. 6. Solitary wave generation in a film 300 Å thick by a heater: (a) surface displacement vs time, (b) temperature change vs time. In (a) and (b) the detector coincides with the heater. (c) superfluid velocity vs time at one edge of the heater. The origin of time is at the instant the heater is turned on.

the propagating modes showed that, for any mode with $n > 34$, the quality factor $Q = \pi$ (decay time/period) was less than 1. (This calls attention to an important feature of our theory, which gives accurate results even when modes having $Q < 1$ are important and also when modes do not vary sinusoidally.) For $n = 2$, the period was $T = 3.7084$ s and the decay time was $\tau = 23.0170$ s. For $n = 4$ the values were $T = 1.8560$ s and $\tau = 5.7543$ s. Higher modes decayed even faster. In the last cycle shown in the figure, only the $n = 2$ mode had an appreciable weight. Therefore, according to the calculations, properties of an essentially pure mode, with $n = 2$, could be observed at times greater than 16 s. This provides a valuable opportunity to study third sound experimentally in its most elementary form. To clarify this point, the contributions to the signal by the sum of the $n = 0$ and 2 modes are also shown in Fig. 8. The effects of the $n = 0$ term do not change in time or space after the excitation pulse is turned off.

B. Waves excited by long bursts of heat

Atkins[4,5] and his collaborators studied third sound on helium films over rectangular horizontal substrates in their pioneering experiments. Waves that propagated along the length of the film were excited by periodically heating a narrow strip for many cycles. During the periodic heating, the thickness of the film was sensed along a line one-quarter of the length from one end.

The measured propagation velocities agreed fairly well with theoretical predictions, as noted in Sec. I. Measured values of attenuation fluctuated widely from day to day, but nevertheless seemed to be much greater than theory predicted. Furthermore, despite substantial effort since then, those and other observed values of attenuation have not yet been explained satisfactorily.

To gain insight into their results, we have applied our more complete theory to the experimental arrangement shown in Fig. 2(c). The length of the substrate was 4.0 cm and the detector was 1.0 cm from one end, just as in the actual experiments[4,5] where attenuation was measured. The linear heater is at the midpoint with respect to length. In this example, the lengths of the heater and detector were taken as 0.01 cm. The temperature was 1.80 K and the depth was 300 Å for the unperturbed film. The vaporization coefficient was $\gamma = 1.0$, and the normal modes $n = 0$–400 were taken into account.

The length of the track is shorter here than in Sec. III A, and so the resonances are now more widely separated in frequency. Therefore, one might expect that properties of individual modes could be more readily observed in this case. Characteristics of the ten lowest normal modes having finite wave numbers are given in Table II. The phase velocity is $c = 76.515$ cm s^{-1} for all the modes shown there. Because of the location of the detectors, they can sense contributions to the surface displacement and temperature change only for even-numbered modes.

Figures 9(a) and 9(b) show the calculated values of surface displacement and temperature change at the detectors when a burst of 10 cycles of sinusoidal power is in-

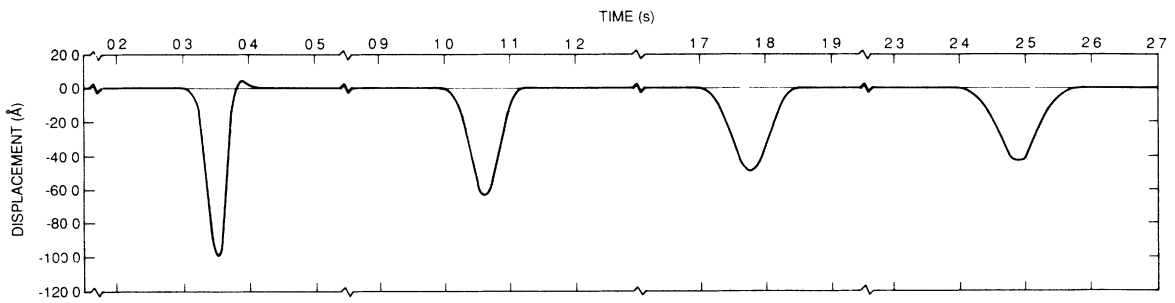

FIG. 7. Solitary waves of third sound in a 1000-Å thick film, showing attenuation and spreading for surface displacement vs time at a fixed detector located one-quarter of the track length from the heater.

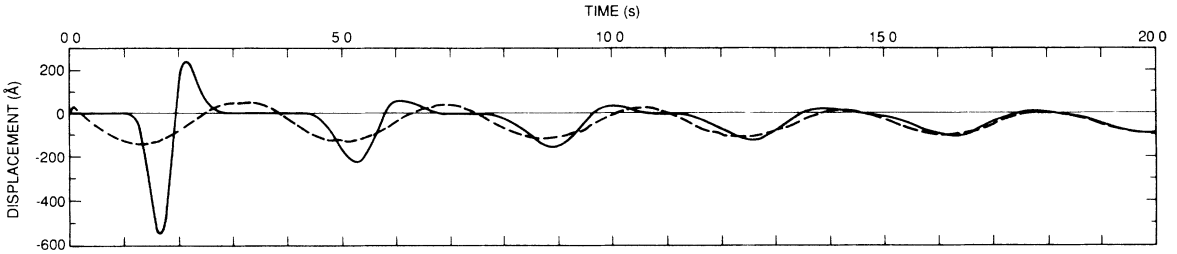

FIG. 8. Third-sound signal in a 3000-Å thick film, excited by a short heat pulse.

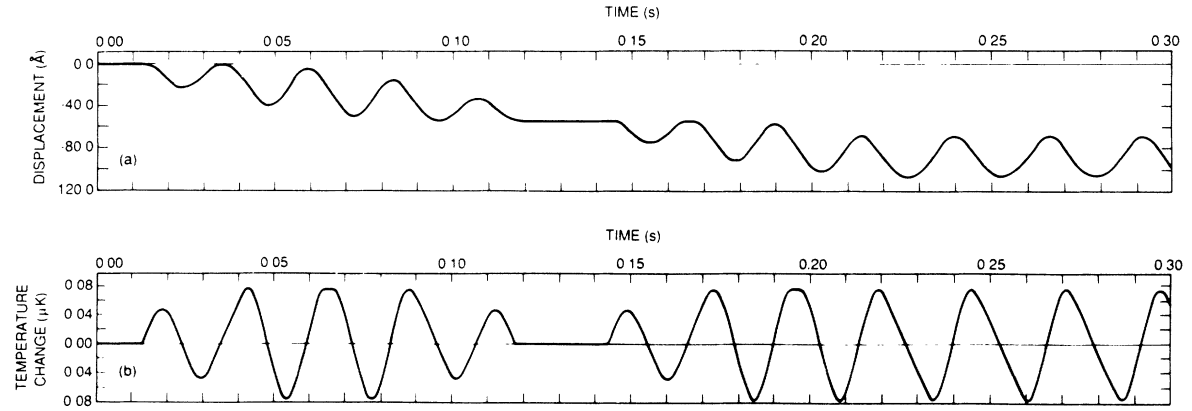

FIG. 9. Third-sound signal in a 300-Å thick film on a horizontal flat plate track with the heater and detector arrangement in Fig. 2(c). Excitation is by a long train of sinusoidal power input at the heater: (a) surface displacement vs time, (b) temperature change vs time.

TABLE II. Calculated properties of normal modes for conditions specified in text with $P = 4.0$ cm.

N	k (cm^{-1})	ω (rad s^{-1})	$\bar{T}$ (s)	τ (s)
1	1.570 80	120.190	$0.522\,770 \times 10^{-1}$	45.770 8
2	3.141 59	240.381	$0.261\,385 \times 10^{-1}$	11.442 7
3	4.712 39	360.571	$0.174\,257 \times 10^{-1}$	5.085 64
4	6.283 19	480.761	$0.130\,692 \times 10^{-1}$	2.860 67
5	7.853 98	600.952	$0.104\,554 \times 10^{-1}$	1.830 83
6	9.424 78	721.142	$0.871\,283 \times 10^{-2}$	1.271 41
7	10.995 6	841.332	$0.746\,814 \times 10^{-2}$	0.934 097
8	12.566 4	961.522	$0.653\,463 \times 10^{-2}$	0.715 168
9	14.137 2	1081.71	$0.580\,856 \times 10^{-2}$	0.565 071
10	15.708 0	1201.90	$0.522\,770 \times 10^{-2}$	0.457 708

serted into the film at the heater. The period of oscillation of heat input was 0.021 7821 s, which is half way between the periods of modes with $n=2$ and 3. The flight time of the earliest discernible displacement signal at the detector is found by calculation to be the same as the travel time at the phase velocity of the low-order modes. The oscillating displacement signal is superimposed on a background of decreasing film thickness for as long as the heater is on, reflecting the net evaporation associated with the $k=0$ mode. Interference effects are prominent between $t=0.118$ and 0.144 s. It may be worth emphasizing here that the $k=0$ mode also contains both steadily decreasing and oscillatory parts and neither of these parts decays exponentially in time or space.

Temperature changes at the detector are shown in Fig. 9(b). Interference effects are also exhibited there. These results show that surface displacement and temperature change are not in antiphase for these waves, implying, for example, that crests are not always colder than troughs, illustrating once again deficiencies in the earlier explanation[1,2] of third-sound structure.

The complexity of the calculated third-sound signals suggests that extraction of meaningful data on attenuation for a plane-wave mode or a normal mode from experiments of this nature would be very difficult and perhaps impossible.

The excitation method used by Atkins[4,5] and coworkers was even more complicated than the one described above. They used a chopped infrared beam to heat the film. To study a more faithful representation of their scheme, we assumed an excitation signal of 10 rectangular pulses. The heater was turned on with constant amplitude for the first half of each cycle and turned off for the other half. The repetition rate was 0.021 7821 s, the same as the period of sinusoidal heating considered in the previous example. All other parameters were the same as for Fig. 9(a). The wave calculated for these conditions is shown in Fig. 10. An oscillating signal superimposed on a background of decreasing film thickness and also interference effects are evident here as for sinusoidal excitation, but now high-frequency ripples add further to the complexity of the wave form and its composition in terms of normal modes. Extraction of information on attenuation for plane waves would be correspondingly more complicated.

In the two examples treated so far in Sec. III B, the heat source was located at the midpoint of the film with respect to its length. Under these circumstances, one could vary the position of the detector and calculate the properties of the film in snapshot form, using the same procedure described in Sec. III A for solitary waves. If one moved the heater to a different location and held it fixed there, the properties of the film could again be viewed in snapshot form. However, the profile of the surface would be different from the previous case because the strength of coupling of the heater to the normal modes depends on the location of the heater with respect to the ends of the substrate. In fact, we have solved this more general problem for an arbitrary location of the heater, and the formulas we found clearly exhibit these features, although we will not give the details here.

In the experiments by Atkins and collaborators, the detector was fixed at one location, about one-quarter of the track length from one end, and the position of the heater was varied stepwise along the track. Each datum point for the surface displacement detector was obtained by integrating over many cycles. They correlated the average of the integrated signals at the detector with the excitation signals and exhibited the data in a form which they interpreted as snapshots of the surface at different instants of time. From those snapshots they inferred values of phase velocity and attenuation for plane waves varying as $e^{i(kx-\omega t)}$. In presenting the data, they assumed x to be the distance between heater and detector. They did not take into account effects of boundary conditions in the normal-mode structure or the location of the heater with respect to the ends of the substrate.

Our analysis above suggests that their interpretation of the experimental data in terms of snapshots of the surface profile is not correct and therefore inferences drawn by them are open to question. Our theoretical model involves an imperfect representation of the actual boundary conditions in their experiment, where the liquid film could be replenished at the ends of the horizontal track. Our theory indicates that, for the long integration times and high power levels which they used, the film would have been thinned substantially unless such replenishment occurred. These effects were, in fact, observed[2] in auxiliary experiments with uninterrupted heating. The accompanying flow would add even greater complexity to the relationship between their experimentally observed signals and plane-wave motion.

For some films, Atkins[5] and collaborators stated that they observed standing waves. Also, in auxiliary experiments,[5] they observed that third sound did not propagate past the edges or ends of a horizontal flat plate where there was a 3-mm step. This suggested[5] that the waves were not able to spread over the edges or ends of the plate in their main experiments on third sound. These results help justify the boundary conditions which we used

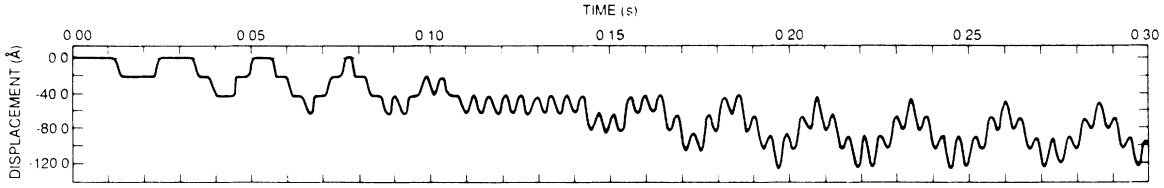

FIG. 10. Third-sound signal in a 300-Å thick film on a horizontal flat plate with the heater and detector arranged as in Fig. 2(c). Excitation is by a long train of rectangular heat pulses, and the detected signal is surface displacement as a function of time.

in modeling their experiments, where we assumed the superfluid velocity was zero at the ends of the horizontal track.

C. Waves excited by short bursts of heat

In our numerical study of third sound so far, we have found that both ultrashort and very long excitation signals usually produce wave forms involving more than one normal mode. In Sec. III C we will examine the region that is intermediate between these extremes. There are two motivations for this study. One is to try to discover circumstances under which individual normal modes of third sound can be excited and investigated systematically, where comparison of experimental observations with theoretical predictions should be particularly transparent. The second is to gain insight into previous experimental studies of propagation velocity and attenuation where short pulses were used. Our numerical work here will be framed in such a way that, to a large extent, both elements are treated at the same time.

Following the lead of the experimenters,[8] we will study third-sound waves excited by a short train of sinusoidal heat input two cycles long. We will also select the other input parameters in our calculations so that they approximate those in the experiments.

Specifically, our theory will be applied to a film on the outer surface of a cylinder, as in Fig. 2(b). The circumference is assumed to be 4.0 cm. (The circumference used in experiments by Wang and Rudnick[8] was 3.2 cm.) A heater is located at the origin $x=0$ and a detector is one-quarter of a circumference away at $x=1.0$ cm. These and other input parameters used in these calculations are the same as in Sec. III B unless it is explicitly stated otherwise. The mathematical description is the same as in Sec. III B even though the shape of the physical apparatus is different. Gravitational effects will be neglected and we will take $\gamma=1.0$ unless it is explicitly stated otherwise.

The same amplitude of power input is assumed in all calculations in Sec. III C, so that it is meaningful to compare the relative strengths of detected signals in Figs. 11–15.

Figure 11 is particularly instructive in studying the modal composition of third sound generated by a short burst of sine waves. The period of the heat input in this case is 0.0174 s, which coincides with the period of the normal mode $n=3$, as one can see in Table II.

The solid curve in Fig. 11 shows the temperature change at the detector that results from excitation of the heater by two full sine waves of power (one full sine wave of voltage across the resistance heater). That curve takes into account the modes $n=0$–400 and is essentially exact within the context of the theory. The flight time of the earliest signal from the heater to the detector is about 0.013 s, corresponding to a velocity of propagation of 76.9 cm s^{-1}. This is very close to the phase velocity of the low-order modes, as one can verify using the data in Table II. The earliest detected signal is nearly sinusoidal for 1.5 cycles and its period is about that of the excitation power, but then there is a null region due to destructive interference when the wave traveling the longer path around the cylinder reaches the detector and combines with that traveling the shorter path. A pattern of sinusoidal temperature change separated by null regions is found for later times also.

A highly significant feature here is that *none* of the detected signal is associated with the $n=3$ normal mode, even though the power input has exactly the same period as that mode. The configuration of heater and detector that we have specified serves as a natural filter in which a detector for temperature change is completely insensitive to odd-numbered modes. One can readily verify this with the aid of Eq. (41). The solid curve in Fig. 11 is due to the combined effects of many even-numbered modes. To exhibit the modal composition of the detected signal in more detail, we have also plotted a curve that takes into account the $n=0$ and 2 modes (dashed line), and another that takes into account the $n=0$, 2, and 4 modes (dot-dashed line). Additional calculations reveal that taking into account all modes through $n=10$ still gives a bad approximation to the exact result when the time is less

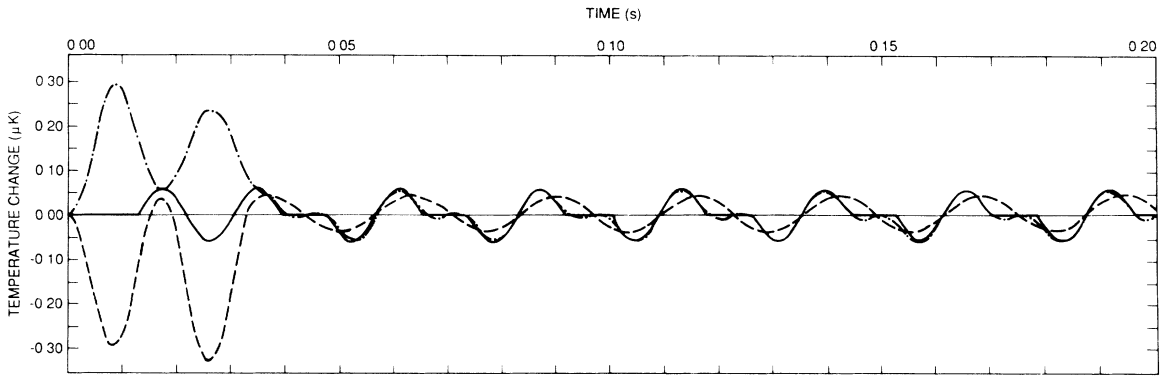

FIG. 11. Third-sound wave in a 300-Å thick film on a cylindrical track with the arrangement of heater and detector shown in Fig. 2(b). Excitation is by a short burst of sinusoidal power input at the heater with the same period as the normal mode $n=3$. The detected signal is for temperature change vs time calculated under the following conditions: (a) —— based on modes $n=0$–400; (b) — — — based on $n=0$ and 2; (c) —·—·—· based on $n=0$, 2, and 4.

than about 0.035 s when the heater is turned off, but gives a good approximation for time greater than this.

The exact theoretical result for the detected temperature change due to waves excited by two cycles of sinusoidal power input at the period of the $n=5$ mode is shown in Fig. 12. The pattern of sinusoidal variations separated by flat regions has many similarities to that shown in Fig. 11. This establishes that the pattern in Fig. 11 is not a unique case for odd modes.

The conditions for studying properties of individual normal modes are more favorable if the excitation power is applied with a period that coincides with that of an even mode. This is illustrated in Fig. 13, where the excitation period coincides with that of the $n=4$ mode. A study of the modal composition of the detected signal shows that the contribution of the $n=4$ mode differs from the exact theoretical result based on the modes $n=0-400$ by less that 0.5% for all times after the excitation power has been turned off, at an elapsed time of 0.026 s. However, a large number of modes contribute to the detected signal while the heater is on. It should be noted that, for this case where $\gamma=1.0$ has been assumed, the $n=4$ mode has a quality factor of over 200, and extraordinary care would be required in an experiment to excite this mode at a frequency within several natural linewidths of the central frequency, where that mode would dominate the detected signal after the excitation power is turned off.

Consider next how these observations are related to existing experimental results. The part of the data reported by Wang and Rudnick[8] for film thicknesses greater than 125 Å has been used to calculate the number of wavelengths that would fit on the circumference of their cylindrical track. Of the several cases we examined, only one corresponded to an index n within one-tenth of an even integer. Two were close to n for odd modes (viz., 2.91 and 3.09), and most of the remaining ones differed from an even integer n by at least 0.3. Since periodic boundary conditions were physically imposed in their experiments, and also since their detector was one-quarter of a circumference from the heater so that odd modes could not be sensed by their detector, one can conclude that those data did not correspond to individual normal modes. Therefore, their assumption that "the train of pulses picked up by the receiver had an exponentially decaying envelope whose time constant gave the attenuation coefficient" appears to be questionable for the thick-film regime which we examined. Only if an individual mode were dominant should one expect simple exponential decay in the time domain, as shown by our theory. In addition, close examination of the only oscillogram of a detected signal in their paper reveals that the envelope is not uniformly decreasing even after the heater is turned off, but exhibits oscillations where the envelope is increasing in some time intervals, typical of complex interfering waves. These observations suggest that quantitative comparison of attenuation rates extracted from their experiments with theoretical results for individual normal modes should be regarded with due reservation. Furthermore, as we have seen in numerical examples, the early part of the detected signal usually has contributions from many normal modes, and so the determination of an attenuation rate for assumed simple exponential decay depends on what part of the detected signal one uses in fitting an envelope because of this effect also.

A film of about 300 Å (80 atomic layers) was the thickest one studied in those experiments,[8] and third-sound attenuation was said to be extremely large there. To us, it seems significant that, for the conditions that existed in those particular measurements, gravity would produce an uneven distribution of equilibrium thickness of the film. Their cylinder was about 1.0 cm in diameter, and calculation shows that film thickness at the top of the cylinder would be about 10% less than at the bottom. This implies that components of the propagating signal having wavelength small compared to the circumference would travel with a velocity at the top of the cylinder that is about 17% greater than at the bottom. Effects of thickness variations for longer wavelengths are not so easy to analyze, but it seems likely that the propagation velocity in a region will just depend on the average depth over a distance of the order of a wavelength. This suggests that, for films of such great thickness, third-sound signals involving at least several normal modes will be distorted due to gravitational effects as they travel around the track.

To study this point further, we developed an iterative solution for a model where third-sound propagates on a film for which the equilibrium thickness varies as a cosine function with one full cycle of variation on the track length. This is a reasonable representation of the horizontal cylinder arrangement in the experiment. Although we have not yet solved those equations numerically, the structure of the equations shows that the uneven equilibrium thickness of the film will affect the shape of the third-sound waves. Also, a study of the equations

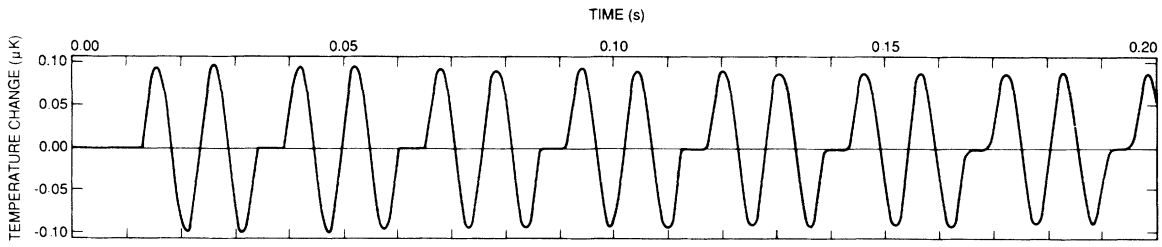

FIG. 12. Third-sound signal calculated for same conditions as in Fig. 11, curve *a*, except that the period of power input in the same as for the normal mode $n=5$.

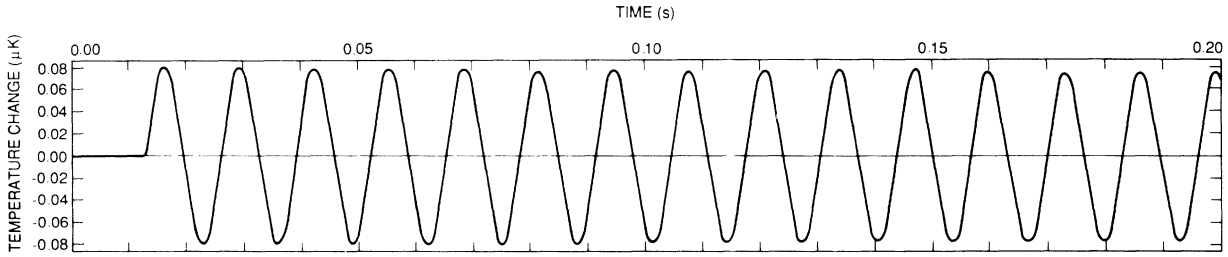

FIG. 13. Third-sound signal calculated for same conditions as in Fig. 11, curve *a*, except that the period of power input is the same as for the normal mode $n=4$.

shows that the wave excited on the uneven film will be affected by the location of the heater, i.e., whether the heater is at a point where the film is thick or thin. Careful attention to this point, particularly for thick films on a cylinder, could be important in obtaining results that are reproducible in different experimental runs.

We have made further calculations to investigate whether our theory could explain the third-sound signals exhibited in the one published oscillogram.[8] The thickness of the film and other important parameters were not reported for that specific case, so we have used the interference pattern as a guide and then varied certain parameters in the theory to search for a match. The theoretical curve in Fig. 14 contains prominent features that are also found in the oscillogram, although the match is not perfect. The period of the two cycles of sinusoidal heat input in this calculation was 0.015 2475 s, midway between the periods for $n=3$ and 4 in Table II. The value of the vaporization coefficient was $\gamma=0.01$, and the calculation took into account the modes $n=0-400$. A study of the modal composition of the wave revealed that even taking into account the lowest modes through $n=100$ was not sufficient to obtain a good approximation to the wave form during the time interval that the heater was turned on. However, after the heater was turned off, near $t=0.030$ s, the $n=2$ and 4 modes, but no others, made important contributions. One should not attach undue significance to the small value of γ (and corresponding high attenuation rate) found here, because we do not know whether the oscillogram was for a thick film, where our theory should be applicable, or for a thin film. However, the calculated results show that the experimental observations are at least compatible with wave forms that can be accounted for by the theory. They also illustrate how the theory can be used in analyzing experiments when the detected signals are not pure modes.

An efficient method of studying properties of some individual normal modes can be distilled from the analysis of third-sound signals treated so far. First consider the case where the detector is a quarter of a track length away from the heater. The track may be annular, cylindrical, or rectangular flat plate. An almost pure $n=2$ mode can be observed by exciting the heater with two cycles of sinusoidal power with a period midway between those of the $n=2$ and 3 modes, or lower, say down to a period midway between those of the $n=1$ and 2 modes. Under these circumstances the $n=4$ mode will have little weight in the excitation signal. Also, the relative positions of the heater and detector guarantee that the odd modes will be filtered out of the detected signal. Time-of-flight methods can be used to determine the propagation velocity. Only the $n=2$ mode is appreciably excited after the heater is turned off, and the envelope of the oscillations can be used to determine the rate of decay for a simple exponential behavior in time.

The dominance of the $n=2$ mode after the heater is turned off near $t=0.0436$ s is exhibited in Fig. 15(a) for the case where the vaporization constant is $\gamma=1.0$. A similar situation exists for $\gamma=0.01$, as illustrated in Fig. 15(b). This provides a practical method for observing the single mode $n=2$ that is useful for a broad range of values of γ and which does not require extraordinary measures in adjusting experimental parameters.

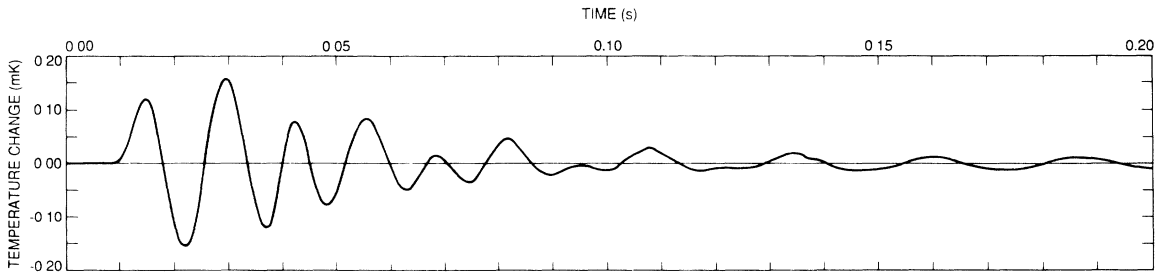

FIG. 14. Third-sound signal calculated for same conditions as in Fig. 11, curve *a*, except that $\gamma=0.01$ and period is midway between that for $n=3$ and 4. The calculated wave form is a close match to that in the oscillogram in Ref. 8.

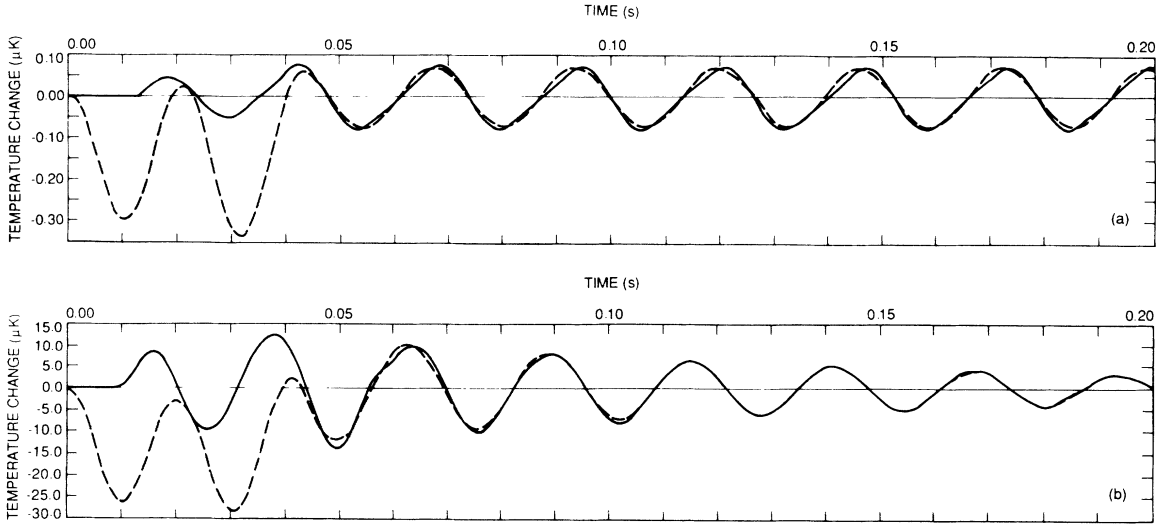

FIG. 15. Third-sound signal for conditions described in the text for period of heat power input midway between that of normal modes $n=2$ and 3. The detected signal is for temperature change vs time calculated under the following conditions: —— based on modes $n=0$–400; — — — based on $n=0$ and 2; (a) $\gamma=1.0$, and (b) $\gamma=0.01$

It can be shown in a similar manner that the $n=1$ mode can be observed almost in isolation by placing a detector one-eighth of a track length from the heater and then exciting the heater at a period fairly close to that for the $n=1$ mode. The specified position of the heater relative to the detector provides a filter that eliminates the $n=2$ mode from the detected signal. The higher-order modes will not be strongly excited and their contributions will decay much sooner than that of the $n=1$ mode, as one finds from an analysis similar to that given earlier for $n=2$. We have calculated the third-sound signal that would be observed in this case when the power input at the heater is two sine waves at a period 1.20 times that of the $n=1$ mode, i.e., at 0.062 732 s for $\gamma=1.0$ and 0.01. The results show that after the heater is turned off, the contribution of the $n=1$ mode to the detected signal differs from the exact theoretical result that takes into account modes $n=1$–400 by about 3% or less.

D. Uniform evaporation

The vaporization coefficient γ is of crucial importance in understanding attenuation in the theory of third sound, and there are still unsettled questions concerning its correct value. This matter will be discussed next. A new method for measuring γ directly, based on uniform evaporation of a film, will then be described.

Much of the beauty and simplicity of Atkins'[1,2] theory is directly related to the assumption that the rate of evaporation depends on γ through Eqs. (10) and (11) when the film is heated slightly above the temperature of the surrounding gas. The equations in Sec. II C show that decay rates for normal modes of third sound are directly proportional to the quantity A in Eq. (46), and A varies inversely with γ.

The term "vaporization coefficient" follows Atkins'[34] terminology most closely in referring to γ in Eq. (11), but other researchers have considered related quantities that they called "condensation coefficient,"[35] "accommodation coefficient,"[36–38] and "coefficient of evaporation."[39] All of these quantities characterize evaporation at a liquid-vapor interface but, in some cases, are defined differently. Even the term "accommodation coefficient" has been defined in different ways by different authors. In some cases it refers to the fraction of incident gas molecules that stick on the surface,[37] but sometimes it refers to effectiveness of energy-transfer processes between molecules in counterflowing streams near the surface.[36] Nevertheless, all of these quantities have sometimes been regarded as equal in discussions in the literature.[37]

Kennard[36] has briefly reviewed work that dates back to the 1800's and which involves these concepts within the context of evaporation from classical liquids. He has also developed simplified derivations of formulas based on those early treatments. Hunter and Osborne[35] have reviewed early work on evaporation from the quantum liquid ^{4}He and developed their own theory as well. Independently, Bergman[10] has developed a theory of evaporation from liquid ^{4}He. Typically, these treatments made assumptions about details of how molecules interact within a few mean free paths of the liquid-vapor interface, details which are hard to substantiate theoretically.

Equally diverse approaches have been used on the experimental side. For example, in evaluating γ for evaporating ^{4}He, Atkins, Rosenbaum, and Seki[34] measured the rate of distillation of bulk liquid near 1 K and inferred $\gamma\approx1$. Hunter and Osborne[35] inferred $\gamma\approx1$ from measurements of the reflection coefficient of second sound from the free surface of liquid He II. Blair and Matheson[38] inferred $10^{-3}\leq\gamma\leq10^{-2}$ from measurements of the period of a torsional oscillator from which an adsorbed helium film was evaporating. Wang *et al.*[37] inferred $\gamma\approx1$ from measurements of the rate of slowing

down of a rotating superconducting sphere levitated in vapor and covered with a saturated helium film.

Each of these experiments was rather indirect and relied on a theoretical formula in order to deduce a value of γ. Because of the difficulties and complexities of both the theoretical and experimental aspects of evaluating γ, we believe that the appropriate value to use in Eq. (11) is still an open question that should be investigated further.

An idealized experiment that can provide a direct, independent evaluation of γ will be described next. The only assumptions involved are already contained in Atkins'[1,2] theory of third sound as we have extended it to include a heat source. Results of this auxiliary experiment could provide values of γ as a function of temperature to be used in theoretical calculations that would permit definitive comparisons with observed properties of third sound, particularly attenuation, which has been so troublesome in the past.

An arrangement for measuring γ is shown in Fig. 16. A thin flat plate is suspended in a horizontal plane by fine fibers. A detector D for measuring thickness of an adsorbed helium film and a thermometer T are located on one face of the plate. The plate has a fairly high electrical sheet resistance, and metallic electrodes are attached to two of its edges so that a uniform electrical current can be passed through it to heat it evenly over its broad surfaces. A film of helium, say about 300 Å thick, is formed on the plate by allowing an attached rod to dip into a bulk liquid reservoir about 2 or 3 cm beneath it. After the film thickness is stabilized, a plunger is used to rapidly lower the level of the reservoir. The switch is then closed and the helium film evaporates uniformly from the surface.

The entire apparatus is positioned near the center of a large cavity whose outer walls are in contact with a helium bath at a steady temperature below T_λ. This fixes the asymptotic temperature boundary condition in the vapor, which is the same as the unperturbed temperature T.

From simultaneous measurements of the film temperature and the time rate of change of the thickness of the adsorbed film, one can determine a unique value of γ. The result does not depend on the film thickness provided that it remains in the range where Atkins' theory is applicable, i.e., greater than about 125 Å.

Calculations based on formulas in Sec. II have been made for a uniformly heated film to illustrate predictions of the theory and show how γ can be evaluated. Our model does not take into account the heat capacity of the film or substrate, and so there is a short transient period after the heater is turned on that is not treated correctly in our calculations. However, following that initial rapid rise in temperature, it levels off at a value that is constant for the remainder of the heating interval. For $\gamma=1.0$, the film thickness will decrease at a steady rate from 300 to 150 Å in 0.500 s when the constant temperature attained by the film is 1.17×10^{-7} K above the unperturbed value of 1.80 K. On the other hand, if one assumes $\gamma=0.01$, the film thickness will decrease at precisely the same rates as for $\gamma=1.0$ when the constant temperature attained by the film is 1.7×10^{-5} K above the unperturbed value of 1.80 K. The rate of evaporation depends only on the heating power input to the film. The steady temperature of the heated film is inversely proportional to γ. One can readily understand this by looking at the $k_n=0$ contribution to the response function $T'(t)$ in Eq. (41) and referring to Eqs. (11), (60b), (62), and (63). Only the $k_n=0$ terms contribute to the response functions under conditions of uniform heating.

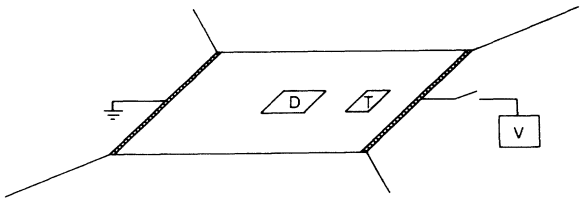

FIG. 16. Arrangement for measuring vaporization coefficient γ based on uniformly heating a helium film adsorbed on a horizontal plate.

In a real experiment, many details must be treated carefully in order to obtain accurate values of γ. Some of the more important ones will be discussed next.

The enclosure should be so large that the atoms evaporated from the film will be only a small fraction of those in the vapor in the unperturbed condition. All support fibers and electrical leads should have very small diameters so that there will be negligible heat flow and liquid flow to or away from the flat plate along them while the heater is on. The flat plate should have a negligible heat capacity so that the film temperature will rise very rapidly when the heater is turned on. The detector D for film thickness should not interfere appreciably with evaporation of the film. A remote measurement of thickness using an optical method utilizing an ellipsometer with low intensity light may be appropriate. However, a comb capacitor may also be satisfactory provided that suitable precautions are taken to minimize its effect on evaporation.

In summary, analysis of an idealized experiment suggests that γ can be measured directly and accurately provided that careful consideration is given to details in a real experiment.

IV. CONCLUSIONS

A powerful tool for investigating properties of third sound has been developed in this article by extending Atkins' theory to include a heat source for excitation. The structure of third sound has been calculated for the first time and the results are inconsistent with earlier views on the subject. Previous interpretations of experimental observations that seemed to indicate major deficiencies in the theory, especially with respect to attenuation, are highly questionable. Additional experiments conducted in accordance with conditions studied in this paper would be useful in resolving these issues and in understanding the newly discovered phenomenon of solitary waves of third sound. The theory indicates that distillation acting in concert with the fountain effect produces the dominant contribution to third-sound attenuation.

ACKNOWLEDGMENTS

We wish to thank Dr. D. M. Strayer for a careful review of the manuscript. The research described in this article was carried out at the Jet Propulsion Laboratory, California Institute of Technology, under contract with the National Aeronautics and Space Administration.

APPENDIX: PHYSICAL PROCESSES IN THIRD-SOUND ATTENUATION

Analysis of attenuation of third sound can be conveniently divided into two parts. First, the terms that account for attenuation in a set of simplified equations for third sound will be identified. Next, an energy-conservation law based on these equations will be derived. Interpretation of that law reveals the physical nature of third-sound attenuation.

The set of simplified equations used in the analysis are obtained by omitting the heat source term in Eq. (15) and keeping only the dominant terms in Eqs. (13), (15), and (17) in accordance with the discussion in Sec. II. From Eq. (13), one finds

$$\rho\frac{\partial\xi}{\partial t}+\rho_s d\frac{\partial v}{\partial x}+KT'=0 . \tag{A1}$$

Equation (15) yields

$$-\rho_s dsT\frac{\partial v}{\partial x}+KLT'=0 . \tag{A2}$$

From Eq. (18) one obtains

$$f\frac{\partial\xi}{\partial x}+\frac{\partial v}{\partial t}-s\frac{\partial T'}{\partial x}=0 . \tag{A3}$$

These three equations can be combined to obtain a single equation for superfluid velocity v as follows. Solve Eq. (A2) for T' and substitute the results in Eq. (A1). This yields

$$\rho\frac{\partial\xi}{\partial t}+\rho_s d\left[1+\frac{Ts}{L}\right]\frac{\partial v}{\partial x}=0 . \tag{A4}$$

Combine Eqs. (A2) and (A3) and obtain

$$f\frac{\partial\xi}{\partial x}+\frac{\partial v}{\partial t}-\rho_s\frac{dTs^2}{KL}\frac{\partial^2 v}{\partial x^2}=0 . \tag{A5}$$

Operate on Eq. (A4) with $f\partial/\partial x$ and on Eq. (A5) with $\rho\partial/\partial t$ and take the difference of the resulting equations. One finds

$$\frac{\partial^2 v}{\partial t^2}-\frac{\rho_s dTs^2}{KL}\frac{\partial^3 v}{\partial x^2\partial t}-f\frac{\rho_s d}{\rho}\left[1+\frac{Ts}{L}\right]\frac{\partial^2 v}{\partial x^2}=0 . \tag{A6}$$

This equation for superfluid velocity can be solved using separation of variables, as follows. Write

$$v(x,t)=V_0(x)V(t) , \tag{A7}$$

substitute Eq. (A7) into (A6) and let k_n^2 be the separation constant. Then V_0 satisfies

$$V_0''+k_n^2V_0=0 , \tag{A8}$$

which has the general solution

$$V_0=V_{01}\cos k_n x+V_{02}\sin k_n x . \tag{A9}$$

The values of k_n can be selected so that either periodic or null boundary conditions are satisfied.

Furthermore, $V(t)$ satisfies

$$\ddot{V}+2Ak_n^2\dot{V}+B_nk_n^4V=0 , \tag{A10}$$

where

$$A\equiv\frac{\rho_s dTs^2}{2KL} \tag{A11}$$

and

$$B_n\equiv\frac{\rho_s fd}{\rho k_n^2}\left[1+\frac{Ts}{L}\right] . \tag{A12}$$

The general solution of Eq. (A10) is

$$V(t)=V_1e^{i\omega_+ t}+V_2e^{i\omega_- t} , \tag{A13}$$

where

$$\omega_\pm=iAk_n^2\pm k_n^2(B_n-A^2)^{1/2} . \tag{A14}$$

From these results, it follows that, when $B_n>A^2$, this normal mode is a simple oscillation in space and a damped oscillation in time with a decay rate per second of Ak_n^2. This is in agreement with results found in Sec. II, as one can see from Eqs. (40), (46), (55), (56b), and (59b).

It is easy to trace the origin of the second term in Eq. (A6), which is responsible for the damping, to the combined effect of the last term in Eq. (A3), which accounts for the fountain effect, and the terms involving K in Eqs. (A1) and (A2), which account for evaporation and condensation. Furthermore, one can easily see that if there were evaporation, but the fountain effect were missing, the second term in Eq. (A6) would be absent and the normal modes would be undamped oscillations in time as well as in space. There also would be no dispersion in this case. This shows that distillation acting alone does not produce third-sound attenuation.

Evaporation and condensation can occur reversibly at a liquid-vapor interface. Also, dissipative coefficients such as viscosity and thermal conductivity do not occur in the set of third-sound equations considered in our development. This raises an interesting question about what process is responsible for converting mechanical motion into heat when third sound is attenuated. The answer can be found with the aid of an energy-conservation law that will be derived next.

Recall that ρ_s is independent of space and time in the approximation we are considering. Multiply Eq. (A3) by $\rho_s v$ and use elementary properties of derivatives of products of two functions and obtain

$$\frac{\partial}{\partial t}(\tfrac{1}{2}\rho_s v^2)=-\rho_s f\frac{\partial}{\partial x}(v\xi)+\rho_s f\xi\frac{\partial v}{\partial x}+\rho_s s\frac{\partial}{\partial x}(vT')-\rho_s sT'\frac{\partial v}{\partial x} . \tag{A15}$$

For a film of width $\overline{W}=1$, integrate Eq. (A15) over the length of the track, from 0 to P, and use the boundary condition that either requires v to be periodic or to vanish at the end points. One finds

$$d\int_0^P \delta x \frac{\partial}{\partial t}(\tfrac{1}{2}\rho_s v^2)=\rho_s f d\int_0^P \delta x\, \xi \frac{\partial v}{\partial x} - \rho_s s d\int_0^P \delta x\, T' \frac{\partial v}{\partial x} . \quad \text{(A16)}$$

Using Eq. (A1), one can rewrite the first term on the right-hand side of Eq. (A16) with the aid of the following results:

$$\begin{aligned}\rho_s d\int_0^P \delta x\, \xi \frac{\partial v}{\partial x} &= \int_0^P \delta x\, \xi(-\rho\xi - KT') \\ &= -\int_0^P \delta x \frac{\partial}{\partial t}(\tfrac{1}{2}\rho\xi^2) - K\int_0^P \delta x T'\xi \\ &= -\int_0^P \delta x \frac{\partial}{\partial t}(\tfrac{1}{2}\rho\xi^2) + \int_0^P \delta x\, \dot{m}_{\text{evap}}\xi .\end{aligned} \quad \text{(A17)}$$

$m=\rho d$ is the mass of the film per unit area and $\dot{m}_{\text{evap}}$ is the time rate of change of m due to evaporation. The relation between $\dot{m}_{\text{evap}}$ and T' can be inferred from Eq. (10).

Next, rewrite the last term in Eq. (A16) with the aid of Eq. (A2):

$$-\rho_s s d\int_0^P \delta x\, T' \frac{\partial v}{\partial x} = -\int_0^P \delta x \left[\frac{L}{T}KT'\right]T' \quad \text{(A18a)}$$

$$= \int_0^P \delta x\, \dot{m}_{\text{evap}} \frac{LT'}{T} . \quad \text{(A18b)}$$

Let $m_s=\rho_s d$ represent the surface superfluid mass density. Combining Eqs. (A16), (A17), and (A18b), and using the fact that limits of integration here do not depend on time so that the time derivative can be taken outside the integral, one obtains

$$\frac{d}{dt}\int_0^P \delta x(\tfrac{1}{2}m_s v^2+\tfrac{1}{2}\rho f\xi^2) = \int_0^P \delta x \left[\dot{m}_{\text{evap}} f\xi + \dot{m}_{\text{evap}}\frac{LT'}{T}\right] . \quad \text{(A19)}$$

Equation (A19) is an energy-conservation law for the whole film. The left-hand side is mechanical energy of the film. The various terms can be interpreted as follows. For a portion of the film of length δx, height $d+\xi$, and width $\overline{W}=1$; $\frac{1}{2}m_s v^2$ is defined as the kinetic energy per unit length due to superfluid motion, $\frac{1}{2}\rho f\xi^2$ is defined as the additional potential energy per unit length acquired by the film due to van der Waals attraction to the substrate when the thickness is changed from d to $d+\xi$. Note that

$$\tfrac{1}{2}\rho f\xi^2 = \int_0^{\xi}(\rho\delta\xi')f\xi' ,$$

where $\rho\delta\xi'$ is mass per unit length of a slab of film of thickness $\delta\xi'$ and unit width, and $f\xi'$, is potential energy per unit mass at level ξ' relative to energy of the film of thickness d. $\dot{m}_{\text{evap}}f\xi$ is defined as the rate at which potential energy enters unit length of a slab of film having unit width due to evaporation of mass at the rate $\dot{m}_{\text{evap}}$. This term may be either positive or negative. $\dot{m}_{\text{evap}}LT'/T$ is defined as the excess rate at which energy enters unit length of the film due to evaporation at the rate $\dot{m}_{\text{evap}}$ when the film is at temperature $T+T'$ instead of T. The energy represented by this last term is associated with irreversible heating of the gas. This term arises from the fountain effect in combination with evaporation, and therefore accounts for third-sound attenuation according to our earlier discussion in this appendix. One can write this term in the following equivalent forms:

$$\begin{aligned}\dot{m}_{\text{evap}}\frac{LT'}{T} &= \dot{m}_{\text{evap}}T'(s_g - s) \\ &= \dot{m}_{\text{evap}}L' = -\frac{KL}{T}(T')^2 .\end{aligned}$$

The middle two members show that this term, which accounts for attenuation, is associated with an excess contribution to the latent heat L'. The last form shows that the term is always negative regardless of whether T' is positive or negative, and this is associated with a correlation between mass flow due to evaporation and the sign of excess latent heat. The negative sign in the last form indicates a decrease of the mechanical energy of the film according to Eq. (A19), and this is in accordance with one's expectations for an attenuation term.

[1] K. R. Atkins, Phys. Rev. **113**, 962 (1959).
[2] K. R. Atkins and I. Rudnick, Prog. Low Temp. Phys. **6**, 37 (1970).
[3] D. J. Bergman, Phys. Rev. A **3**, 2058 (1971).
[4] C. W. F. Everitt, K. R. Atkins, and A. Denenstein, Phys. Rev. Lett. **8**, 161 (1962).
[5] C. W. F. Everitt, K. R. Atkins, and A. Denenstein, Phys. Rev. **136**, A1494 (1964).
[6] I. Rudnick, R. S. Kagiwada, J. C. Fraser, and E. Guyon, Phys. Rev. Lett. **20**, 430 (1968).
[7] D. J. Bergman, in *Physical Acoustics*, edited by W. P. Mason and N. Thurston, (Academic, New York, 1975), Vol. XI, Chap. 1.
[8] T. G. Wang and I. Rudnick, J. Low Temp. Phys. **9**, 425 (1972).
[9] B. Ratnam and J. Mochel, Phys. Rev. Lett. **25**, 711 (1970).
[10] D. Bergman, Phys. Rev. **188**, 370 (1969).
[11] B. Ratnam and J. Mochel, J. Low Temp. Phys. **3**, 239 (1970).
[12] B. Ratnam and J. Mochel, *Proceedings of the International Conference on Low Temperature Physics—LT-13, Boulder, 1972*, edited by K. D. Timmerhaus, W. J. O'Sullivan, and E. F. Hammel (Plenum, New York, 1974), Vol. I, p. 233.
[13] E. R. Generazio and R. W. Reed, J. Low Temp. Phys. **57**, 501 (1984).
[14] C. G. Kuper, Physica **22**, 1291 (1956).
[15] L. D. Landau, J. Phys. (U.S.S.R.) **5**, 71 (1941); **11**, 91 (1947). These papers are included as reprints in Ref. 16.
[16] I. M. Khalatnikov, *Introduction to the Theory of Superfluidity* (Benjamin, New York, 1965), pp. 6 and 7.

[17]K. A. Pickar and K. R. Atkins, Phys. Rev. **178**, 389 (1969).
[18]R. S. Kagiwada, J. C. Fraser, I. Rudnick, and D. Bergman, Phys. Rev. Lett. **22**, 338 (1969).
[19]J. M. Kosterlitz and D. J. Thouless, J. Phys. C **5**, L124 (1972).
[20]J. M. Kosterlitz and D. J. Thouless, J. Phys. C **6**, 1181 (1973).
[21]J. M. Koterlitz, J. Phys. C **7**, 1046 (1974).
[22]D. R. Nelson and J. M. Kosterlitz, Phys. Rev. Lett. **39**, 1201 (1977).
[23]I. Rudnick, Phys. Rev. Lett. **40**, 1454 (1978).
[24]K. L. Telschow and R. B. Hallock, Phys. Rev. Lett. **37**, 1484 (1976); R. K. Galkiewicz, K. L. Telschow, and R. B. Hallock, J. Low Temp. Phys. **26**, 147 (1977); D. T. Ekholm and R. B. Hallock, Phys. Rev. Lett. **42**, 449 (1979).
[25]K. Telschow, I. Rudnick, and T. G. Wang, J. Low Temp. Phys. **18**, 43 (1975); D. T. Ekholm and R. B. Hallock, *ibid.* **42**, 339 (1981).
[26]V. M. Kontorovich, Zh. Eksp. Teor. Fiz. **30**, 805 (1956) [Sov. Phys. JETP **3**, 770 (1956)].
[27]H. V. Verbeek, E. Van Spronsen, H. Mars, H. Van Beelan, R. De Bryn Ouboter, and K. W. Taconis, Physica **73**, 621 (1974).
[28]G. M. Graham and E. Vittoratos, Phys. Rev. Lett. **33**, 1136 (1974).
[29]H. W. Jackson, Phys. Rev. B **19**, 2556 (1979).
[30]P. V. Mason, D. Petrac, D. D. Elleman, T. Wang, H. W. Jackson, D. J. Collins, P. J. Cowgill, and J. R. Gatewood, in *Proceedings of ICEC 11, Berlin, 1986,* edited by G. Klipping and I. Klipping (Butterworth, United Kingdom, 1986).
[31]F. London, *Superfluids Vol. II, Macroscopic Theory of Superfluid Helium* (Dover, New York, 1964), Secs. 19 and 20.
[32]J. Wilks, *The Properties of Liquid and Solid Helium* (Oxford University Press, London, 1967), p. 412.
[33]L. D. Landau and E. M. Lifshitz, *Statistical Physics* (Addison-Wesley, Reading, Mass., 1958), pp. 71 and 72.
[34]K. R. Atkins, B. Rosenbaum, and H. Seki, Phys. Rev. **113**, 751 (1959).
[35]G. H. Hunter and D. V. Osborne, J. Phys. C **2**, 2414 (1969).
[36]E. H. Kennard, *Kinetic Theory of Gases* (McGraw-Hill, New York, 1938), p. 311.
[37]T. G. Wang, D. D. Elleman, E. E. Olli, and M. M. Saffren, Phys. Rev. Lett. **30**, 485 (1973).
[38]D. G. Blair and C. C. Matheson, *Proceedings of the 13th International Conference on Low Temperature Physics—LT-13, Boulder, 1972,* Ref. 12, Vol. I, p. 190.
[39]E. H. Kennard, *Kinetic Theory of Gases,* Ref. 36, p. 69.

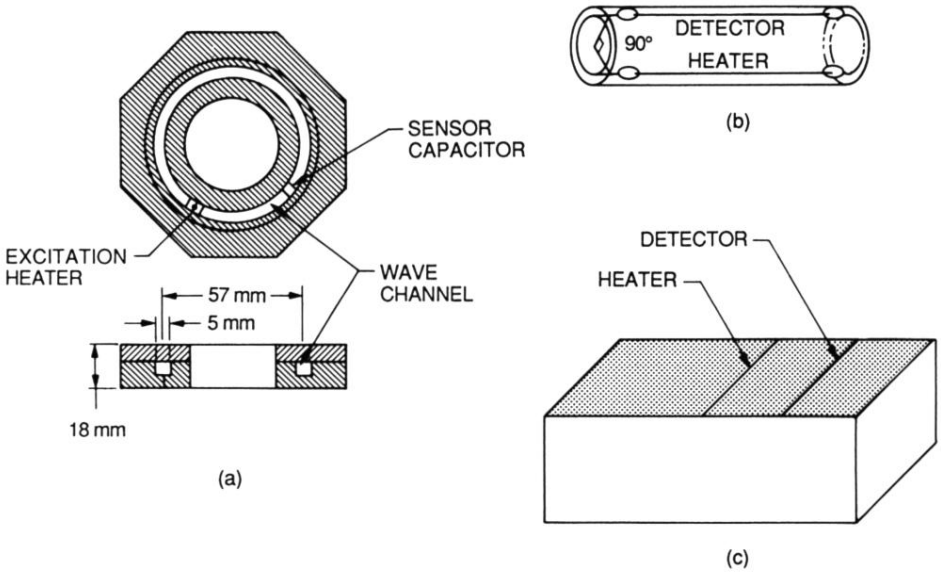

FIG. 2. Tracks for third-sound waves: (a) annular channel, (b) cylinder surface with horizontal axis, (c) horizontal flat plate.